Enzyme Architecture: The Effect of Replacement and Deletion Mutations of Loop 6 on Catalysis by Triosephosphate Isomerase[‡]

Xiang Zhai,[1] Maybelle K. Go,[1] AnnMarie C. O'Donoghue,[2] Tina L. Amyes,[1] Scott D. Pegan,[3] Yan Wang,[4] J. Patrick Loria,[4,5] Andrew D. Mesecar,[6] and John P. Richard[1,*,†]

[1] *Department of Chemistry, University at Buffalo, Buffalo, NY, 14221*

[2] *Department of Chemistry, Durham University, Durham, DH1 3EL, UK*

[3] *Department of Pharmaceutical and Biomedical Sciences, University of Georgia, Athens, GA 30602*

[4] *Department of Chemistry, Yale University, New Haven, CT 06520*

[5] *Department of Chemistry and Molecular Biophysics and Biochemistry, Yale University, New Haven, CT 06520*

[6] *Departments of Biological Sciences and Chemistry, Purdue University, West Lafayette, IN 47907*

[‡]This work was supported by Grant GM 39754 from the National Institutes of Health to JPR and MCB1121372 from the National Science Foundation to JPL.

* Author to whom correspondence should be addressed

Tel: (716) 645 4232

Fax: (716) 645 6963

Email: jrichard@buffalo.edu

Running Title: Loop 6 Mutations of TIM

ABBREVIATIONS

TIM, triosephosphate isomerase; *c*TIM triosephosphate isomerase from chicken muscle; DHAP, dihydroxyacetone phosphate; GAP, (*R*)-glyceraldehyde 3-phosphate; *d*-DHAP, [1(*R*)-^{2}H]-dihydroxyacetone phosphate; *d*-GAP, [2(*R*)-^{2}H]-glyceraldehyde 3-phosphate; TEA, triethanolamine; MES, 2-(N-morpholino)ethanesulfonic acid; MG, methylglyoxal; GA, glycolaldehyde; PGA, 2-phosphoglycolate; HP_i, phosphite dianion; PGH, phosphoglycolohydroxamate; L6RM, loop 6 replacement mutant; NADH, nicotinamide adenine dinucleotide, reduced form; NAD^+, nicotinamide adenine dinucleotide, oxidized form; NMR, nuclear magnetic resonance; OMPDC, orotidine 5'-monophosphate decarboxylase; G3P, glycerol-3-phosphate.

ABSTRACT: Two mutations of the phosphodianion gripper loop in chicken muscle triosephosphate isomerase (*c*TIM) were examined: (1) the loop deletion mutant (LDM) formed by removal of residues 170-173 [(1990) *Biochemistry 29*, 3186-3194]; (2) the loop 6 replacement mutant (L6RM), where the N-terminal hinge sequence of TIM from eukaryotes, 166-PXW-168 [X = L, V], is replaced by the sequence from archae, 166-PPE-168. The X-ray crystal structure of the L6RM shows is a large displacement of the side chain of E168 from that for W168 at wild type *c*TIM. Solution NMR data show that the L6RM results in significant changes in chemical shift at loop 6 and surrounding regions, and that the binding of glycerol 3-phosphate (G3P) results in smaller changes in the chemical shift for nuclei at the active site of the L6RM compared with wild type *c*TIM. Interactions with loop 6 of the L6RM stabilize the enediolate intermediate towards the elimination reaction catalyzed by for the LDM. The LDM and L6RM result in 800,000 and 23,000-fold decreases, respectively, in k_{cat}/K_m for isomerization of GAP. Saturation of the LDM, *but not the L6RM*, by substrate and inhibitor phosphoglycolate is detected by steady-state kinetic analyses. We propose, based upon a comparison of X-ray crystal structures for wild type TIM and the L6RM, that ligands bind weakly to the L6RM because a large fraction of the ligand binding energy is utilized to overcome destabilizing electrostatic interactions between the side chains of E168 and E129 that are predicted to develop at the loop-closed enzyme. Similar normalized yields of DHAP, *d*-DHAP and *d*-GAP are formed in LDM- and L6RM-catalyzed reactions of GAP in D_2O. The smaller normalized 12 – 13% yield of (DHAP + *d*-DHAP) observed for the mutant *c*TIM-catalyzed reactions compared with the 79% yield of these products for wild type *c*TIM suggests that these mutations impair proton transfer from O-2 to O-1 at the initial enediolate phosphate intermediate. No products are detected for the LDM-catalyzed isomerization reactions in D_2O of [1-^{13}C]-GA and HP_i, but the L6RM-catalyzed reaction in the presence of 0.020 M dianion gives a 2% yield of the isomerization product [2-^{13}C, 2-^{2}H]-GA.

Triosephosphate isomerase (TIM) appeared early in evolution as an enzyme that catalyzes a step in glycolysis, a universal metabolic pathway.[1] TIM catalyzes the stereospecific and reversible conversion of dihydroxyacetone phosphate (DHAP) to (*R*)-glyceraldehyde 3-phosphate (GAP),[2,3] by proton transfer reactions at carbon, through enzyme-bound *cis*-enediolate reaction intermediates (Scheme 1). Intramolecular proton transfer between C-1 and C-2 is carried out by the carboxylate side-chain of Glu165, [4-8] and the neutral electrophilic imidazole side-chain of His-95 plays a role in mediating proton transfer between O-1 and O-2 of the enediolate.[9-11] We are interested in understanding the mechanism of action of TIM, and are intrigued by the repeating flexible loops at the archetypal TIM barrel.[12-15] There is the strong probability that the properties of these loops are well adapted for catalytic strategies perfected by TIM early in evolution.[15-17] At least one strategy, the utilization of phosphodianion binding energy for catalysis,[18] has been widely observed for enzymes that catalyze a variety of reactions including, decarboxylation,[19] proton transfer,[20] hydride transfer,[21] phosphoryl transfer,[22] and a more complex reaction.[23]

Scheme 1

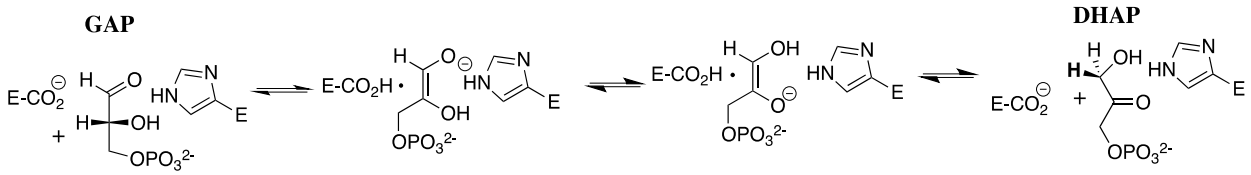

The 11-residue flexible loop 6 of TIM (Scheme 2) is open in unliganded TIM, to allow substrate free access to the active site.[14,24] Binding of DHAP to TIM triggers closure of loop 6 over the substrate phosphodianion and formation of the "caged" enzyme-PGA complex shown in Figure 1A.[15,16] The alkyl ammonium side chain of K12 stretches across the protein surface towards the base of loop 6, and forms a solvent-separated ion pair with the phosphodianion. The

side chain of K12 is anchored to the protein surface by an ion pair with the carboxylate side chain of E97:[25] its deletion results in a 10^5 -falloff in k_{cat}/K_m for the K12G mutant of TIM from yeast.[26,27] Two lines of evidence show that the interactions between loop 6 and dianions activate TIM for deprotonation of bound carbon acid substrates.

Scheme 2

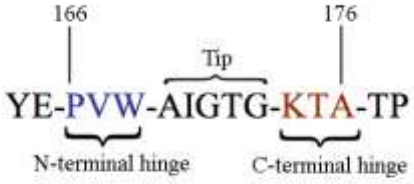

(1) Deletion of residues 170-173 from loop 6 of TIM from chicken muscle (*c*TIM), and introduction of a peptide bond between A169 and K174 disrupts loop-dianion interactions, but should leave the protein fold unaffected (Figure 1B).[28] This loop deletion mutation (LDM) results in a 10^5-fold decrease in k_{cat}, but only a 5-fold increase in K_m for isomerization of GAP.[28] This shows that the strong stabilizing interactions between loop 6 and the ligand are *only* expressed at the transition state for the isomerization reaction. Interactions between loop 6 and the enediolate phosphate intermediate play the additional vital role of suppressing the breakdown of the intermediate to form methylgloxal and inorganic phosphate,[28-30] the dominant nonenzymatic reaction of triosephosphates in water.[31]

(2) Cutting the connection between the carbon acid and phosphodianion of GAP allows the examination of the effect of TIM-dianion interactions on the catalytic activity.[17,32] We have shown that the binding of phosphite dianion to TIM results in a large increase in the enzymatic activity, as measured by the increase in the apparent second-order rate constant $(k_{cat}/K_m)_{obs}$ for the TIM-catalyzed deuterium exchange reactions of truncated substrates glycolaldehyde (GA),[32] and [1-^{13}C]-GA in D_2O.[33] Phosphite dianion activation of enzyme-catalyzed proton transfer and

decarboxylation reactions catalyzed by orotidine 5'-monophosphate decarboxylase,[19,20,34,35] and for the hydride transfer reaction catalyzed by glycerol 3-phosphate dehydrogenase have also been observed.[21]

Loop 6 pivots around the N-terminal (PVW) and the C-terminal (KTA) hinges during loop closure, while the "tip" residues (AIGTG) move as a rigid body (Scheme 2).[36] The loop-open and closed forms of TIM were characterized by solid state NMR,[37-39] solution NMR,[40,41] and temperature jump fluorescence spectroscopy studies,[42] where it was concluded that loop-opening and closing is *just* sufficiently fast to account for TIM-catalyzed turnover of substrate. Studies on mutants at hinge residues show that substitution of glycine in these positions results in a falloff in catalytic activity.[43,44] It was proposed that the Gly mutations result in an increase in the number of protein conformations for the flexible loop-open form of TIM, which provides an entropic stabilization of the unliganded open enzyme compared with the rigid closed form of TIM.[45,46]

We report here the results of experiments on the loop 6 deletion mutant (LDM),[28] and of a loop 6 replacement mutant (L6RM), where the N-terminal hinge sequence of TIM from eukaryotes and bacteria, 166-PXW-168 [X = L, V], is replaced by the sequence found in archae, 166-PPE-168.[47] These include: (a) Steady state kinetic and inhibition studies; (b) X-ray crystallographic and solution NMR structural data for the L6RM; (c) The products of the mutant *c*TIM-catalyzed reactions of GAP in D_2O;[48-50] (d) Kinetic and product data for the mutant TIM-catalyzed reactions of [1-^{13}C]-GA in D_2O in the absence and presence of phosphite dianion.[32,33] We show that the LDM serves as a benchmark for catalysis, where there is little or no stabilization of the transition state for TIM-catalyzed isomerization by interactions with loop 6. This assists in the development of a structure-based interpretation of the effect of the L6RM on

TIM-catalyzed isomerization reactions.

MATERIALS AND METHODS

Rabbit muscle glycerol 3-phosphate dehydrogenase and glyceraldehyde 3-phosphate dehydrogenase were purchased from Sigma. Bovine serum albumin (BSA) and protease inhibitor tablets (Complete®) were purchased from Roche. DEAE-Sepharose, DEAE-Sepharose FF, and DEAE-Sephadex were from GE Healthcare. D,L-Glyceraldehyde 3-phosphate diethyl acetal (barium salt), glycerol-3-phosphate (powder), dihydroxyacetone phosphate (magnesium salt), NADH (disodium salt), dithiothreitol (DTT), Dowex 50WX4-200R, triethanolamine hydrochloride (TEA·HCl), sodium deuteroxide (40 wt%, 99.5% D) and imidazole were purchased from Sigma. NAD (free acid) was purchased from MP Biomedicals. Sodium phosphite (dibasic, pentahydrate) and sodium hydrogen arsenate (heptahydrate) were from Fluka. [1-^{13}C]-Glycolaldehyde ([1-^{13}C]-GA) 99% enriched at C-1 with carbon-13 was purchased from Omicron Biochemicals as a 0.09 M solution in water. Deuterium oxide (99% D), deuterium chloride (35 wt%, 99.9% D), $^{15}NH_4Cl$ and [$^{13}C_6$]-glucose were from Cambridge Isotope Laboratories. 2-Phosphoglycolic acid was prepared by a literature procedure.[51] The disodium salt of D-glyceraldehyde 3-phosphate diethyl acetal was prepared by a literature procedure,[52] and purified by column chromatography over DEAE-Sephadex. Imidazole was recrystallized from benzene. Water was from a Milli-Q Academic purification system. All other chemicals were reagent grade or better and were used without further purification. The methods for the preparation of solutions and for all enzyme assays in 30 mM TEA buffer, pH 7.5, I = 0.1 (NaCl) and at 25 °C were described in a recent publication.[53]

Preparation of Enzymes. Wild type *c*TIM was prepared as described in earlier work,[53] using the expression vector pET-15b.[33] This plasmid was introduced into the TIM-deficient *tpi*A$^-$

□DE3 lysogenic strain of *E. coli*, FB215471(DE3),[53,54] and the enzyme was expressed and purified according to published procedures.[43,53] The concentration of TIM subunits was determined from the UV absorbance at 280 nm using the extinction coefficient of 33460 M^{-1} cm^{-1} that was calculated from the ProtParam tool available on the Expasy server.[55]

Loop 6 Replacement Mutant (L6RM). The expression vector pET-15b that contained the gene encoding wild type *c*TIM was used to prepare the 167-VW-168 to 167-PE-168 mutant. The mutation was completed in a single mutagenesis step using primers 5'- GGTTCTTGCCTATGA GCCACCAGAAGCTATCGGAACTGGTAAAACTGC -3' (sense) and 5'- GCAGTTTTACCA GTTCCGATAGCTTCTGGTGGCTCATAGGCAAGAACC -3' (antisense) and the wild type plasmid as the cloning template. The sequence of the plasmid strands was confirmed by DNA sequencing. This plasmid was then introduced into the TIM-deficient *tpi*A$^-$ □DE3 lysogenic strain of *E. coli*, FB215471(DE3).[53] For NMR and crystallography experiments wild type and mutant TIM enzymes were expressed in *E. coli* BL21 (DE3) cells. The loop 6 replacement mutant enzyme was expressed and purified using the procedures described for wild type *c*TIM.[43,53] The concentration of TIM subunits was determined from the UV absorbance at 280 nm using the extinction coefficient 27960 M^{-1} cm^{-1} that was calculated from the ProtParam tool available on the Expasy server.[55]

Loop 6 Deletion Mutant (LDM). The plasmid pBSX1cTIM, containing the wild-type gene of *c*TIM,[56] and *E. coli* strain DF502 (strep^R, tpi$^-$, and his$^-$), whose DNA lacks the gene for TIM,[57] were generous gifts from Professor Nicole Sampson. The loop 6 deletion mutation was introduced into pBSX1cTIM in two steps by PCR mutagenesis using the Quick Change™ mutagenesis kit. A *Bsi* WI restriction site was first constructed by site-directed mutagenesis using the following primers to change the wild type sense sequence from CTAT to GTAC and

the antisense sequence from GATA to CATG: 5'-GTAAGGTGGTTCTTGCGTACGAGCCAGTTTGGGCTATC-3' (sense) and 5'-GATAGCCCAAACTGGCTCGTACGCAAGAACCACCTTAC-3' (antisense). The restriction site in this plasmid, pBS09, was used to construct plasmid pBS10 for the loop 6 deletion mutant. The following primers were synthesized: 5'-GTACGAGCCAGTTTGGGCTAAAACTGCTACTCCCCAACAGGCTCAGG AGGTTCATGAGAAGCTGAGAGGCTGGCTCAAAAGCCAC-3' (sense) and 5'-GTGGCTTTTGAGCCAGCCTCTCAGCTTCTCATGAACCTCCTGAGCCTGTTGGGGAG TAGCAGTTTTAGCCCAAACTGGCTC-3' (antisense). The sense primer was complementary to bases 489-507 and 520-585 of the gene for wild-type *c*TIM and was designed to delete the bases 508-519 that code for residues 170-173 of *c*TIM. The sequence of each constructed plasmid strand was confirmed by sequencing. The LDM of *c*TIM was expressed and purified by following procedures developed for wild type *c*TIM.[33,43] The concentration of TIM subunits was determined from the UV absorbance at 280 nm using the extinction coefficient of 33460 M^{-1} cm^{-1} that was calculated from the ProtParam tool available on the Expasy server.[55]

Isotope-labeled L6RM for NMR studies. A sterile scraping of plasmid glycerol stock was used to inoculate a starter culture in LB rich medium, which was grown to mid log phase. A small amount of this culture was diluted 200-fold into M9 minimal medium [0.4% (w/v) glucose] in 50% D_2O) and the cells were grown overnight. This entire culture was then transferred to 1 L of M9 minimal medium in 99% D_2O and grown to an OD_{600} of 0.6-0.8, at which point 0.8 mM IPTG was added to induce protein expression at 30 °C. When necessary, uniform isotopic labeling of TIM with ^{15}N and ^{13}C was achieved using $^{15}NH_4Cl$ and [$^{13}C_6$]-glucose as the nitrogen and carbon sources, respectively. Cells were harvested by centrifugation

after 16 to 18 h of induction and then stored frozen at -80 °C.

The frozen *E. coli* pellet was thawed on ice and then lysed by two cycles of sonication in 10 mM Tris-HCl buffer at pH 7.5 in the presence of 1 mM protease inhibitor phenylmethylsulfonyl fluoride. The lysed cell culture was clarified by centrifugation at 20,000 g, and Benzonase (Novagen) added to give a final level of 25 unit/ml lysate. The crude lysate was loaded onto a DEAE-Sepharose FF weak ion-exchange column and eluted with the same buffer and a linear concentration gradient of KCl from 0 to 60 mM over a total volume of 400 mL at a flow rate of 2 mL/min. Fractions containing cTIM were pooled and desalted using an Amicon Centriprep Concentrator with a MWCO of 10,000 kDa. The desalted sample was loaded onto the DEAE- Sepharose FF column a second time to remove minor contaminants and remaining traces of DNA. *c*TIM eluted from this second column in a single elution peak centered at a salt concentration of about 12 mM. The final eluted fractions containing cTIM and determined to be more than 95% pure were pooled and dialyzed against appropriate buffers, concentrated and stored at 4 °C. The final protein yields were between 30-50 mg from 1 L of growth.

X-ray Crystal Structure Determination. The initial conditions for crystallization of the L6RM of *c*TIM were determined using Hampton Research Index HT, Crystal Screen HT and SaltRx HT screens. The final crystals were grown by the hanging-drop vapor diffusion method at room temperature. The crystallization drops included 2 μL of a 35.9 mg/mL solution of the L6RM of *c*TIM in 10 mM 2-(N-morpholino)ethanesulfonic acid at pH 6.60, 10 mM sodium chloride, 0.02% sodium azide mixed in a 1:1 ratio with a precipitant of 26% PEG 3350 and 0.1 M Tris, pH 8.5. The typical crystal size was 0.1 - 0.2 mm.

The X-ray data set for the L6RM of *c*TIM was collected at the SER-CAT beam line 22-ID. The crystal was mounted on nylon loops and submerged in a 5 μL volume of 30% PEG 3350

and 0.1 M Tris, pH 8.5 as a cryo solution. Crystals were subsequently flash-cooled in liquid nitrogen and mounted under a stream of dry N_2 at 100 K. The data set was collected using a MAR 300 CCD detector. X-ray images were indexed, processed, integrated and scaled together using the program HKL2000.[58] The data set for the L6RM revealed a C2 space group. Initial phases were readily obtained using Phaser and wild type *c*TIM (1TPH) as a starting model.[59] The program WinCoot was used for model building, and Refmac 5.8 from the CCP4 suite was used for refinement.[60] Anisotropic temperature factors were refined and occupancies were 1.00 for all atoms. Water molecules were added to F_o-F_c density peaks that were greater than 3σ using the "Find Water" WinCoot program function. The final models were checked for structural quality using the CCP4 suite programs Procheck and Sfcheck. The atomic coordinates and structure factors have been deposited with the Protein Data Bank (PDB code 4P61).

^{1}H NMR Product Analyses. ^{1}H NMR spectra at 500 MHz were recorded in D_2O at 25 °C using a Varian Unity Inova 500 spectrometer that was shimmed to give a line width of ≤ 0.7 Hz for each peak of the doublet due to the C-1 proton of GAP hydrate, or ≤ 0.5 Hz for the most downfield peak of the double triplet due to the C-1 proton of [1-^{13}C]-GA hydrate. Spectra (16-64 transients) were obtained using a sweep width of 6000 Hz, a pulse angle of 90°, an acquisition time of 6 s and a relaxation delay of 60 s ($4T_1$) for experiments on the TIM-catalyzed isomerization of GAP in D_2O or 120 s ($> 8T_1$) for experiments on the TIM-catalyzed reactions of [1-^{13}C]-GA in D_2O.[33,50] Baselines were subjected to a first-order drift correction before determination of peak areas. Chemical shifts are reported relative to HOD at 4.67 ppm.

Steady-State Kinetic Parameters. Values of k_{cat} and K_m for the LDM *c*TIM-catalyzed isomerization of GAP (0.075 – 11 mM) in solutions that contain 30 mM TEA buffer, pH 7.5, I = 0.1 (NaCl) and at 25 °C were determined from the nonlinear least squares fit of the initial

velocity data to the Michaelis-Menten equation. Arsenate (10 mM) was used as an activator for glyceraldehyde 3-phosphate dehydrogenase, the coupling enzyme in our assay for the L6RM-catalyzed isomerization of DHAP (0.08 – 20 mM). A control experiment showed that there is no detectable inhibition of the L6RM *c*TIM-catalyzed reaction by 10 mM arsenate. Inhibition of the L6RM-catalyzed reaction of GAP in the presence of 2-phosphoglycolate (PGA, 1 – 10 mM) was examined at pH 7.5 (I = 0.1, NaCl) by determining values of k_{cat}/K_m from the slopes of linear correlations of 4 – 5 values of v_i/[E] against [GAP] for reactions at several different [PGA].

Mutant *c*TIM-Catalyzed Isomerization of GAP in D_2O. The LDM and L6RM of *c*TIM were exhaustively dialyzed at 7 °C against 30 mM imidazole (70% free base) in D_2O at pD 7.9 and I = 0.1 (NaCl). The reaction in a volume of 750 μL was initiated by addition of enzyme to the reaction mixture containing GAP, imidazole buffer (pD 7.9) and NaCl in D_2O to give final concentrations of 10 mM GAP, 10 mM imidazole (70% free base, I = 0.1 (NaCl)) and 0.4 μM L6RM or 7 μM LDM. Spectra (12 transients) were recorded continuously for a period of 2 – 4 h, during which time > 80% of GAP was converted to products. In all experiments, the fraction of the remaining substrate GAP (f_{GAP}) and the fraction of GAP converted to products DHAP (f_{DHAP}), *d*-DHAP ($f_{d\text{-}DHAP}$), *d*-GAP ($f_{d\text{-}GAP}$) and methylglyoxal (MG, f_{MG}) at time t were determined from the integrated areas of the appropriate ^{1}H NMR signals, as described in earlier work.[50] The peak areas were normalized using the invariant signal for the C-(4,5) protons of imidazole as an internal standard.[50]

Reaction of [1-^{13}C]-GA in D_2O. The enzymes were exhaustively dialyzed at 7 °C against 30 mM imidazole (20% free base) in D_2O at pD 7.0 and I = 0.1 (NaCl) or I = 0.024, for reactions in the absence or the presence of 40 mM total phosphite, respectively. The reaction in the absence of HP_i was initiated by addition of enzyme to a mixture, which contains [1-^{13}C]-GA,

imidazole and NaCl in D_2O to give final concentrations of 20 mM [1-^{13}C]-GA, 20 mM imidazole at pD 7.0 (I = 0.1, NaCl), and 0.32 mM LDM or 0.39 mM L6RM of *c*TIM in a volume of 850 μL. The reactions in the presence of HP_i at 25 ºC and I = 0.1 (NaCl) were initiated by addition of enzyme to a mixture, which contains 20 mM [1-^{13}C]-GA, 40 mM phosphite (50% dianion, pD 7.0), 10 mM imidazole at pD 7.0, and 0.32 mM LDM of *c*TIM or 0.23 mM L6RM of *c*TIM in D_2O in a volume of 850 μL. In each case 750 μL of the reaction mixture was transferred to an NMR tube. The NMR spectrum was recorded immediately and then at regular intervals over a period of several days. After collection of the final spectrum, the protein was removed by ultrafiltration and the pD was determined. There was no significant change in pD (≤ 0.03 unit) during these reactions. The remaining reaction mixture was incubated at 25 °C and used to monitor the TIM activity. The enzymatic activity was unchanged during the time for these experiments. These reactions were monitored for the disappearance of [1-^{13}C]-GA and for the formation of reaction products (Chart 1), as described in previous work.[33] Observed first-order rate constants, k_{obs} (s^{-1}), for the disappearance of [1-^{13}C]-GA were determined from the slope of linear semilogarithmic plots of the reaction progress against time (eq 1), where f_s is the fraction of [1-^{13}C]-GA that remains at time t. The observed second-order rate constant, $(k_{cat}/K_m)_{obs}$, was determined from the values of k_{obs} using eq 2, where f_{hyd} = 0.94 is the fraction of [1-^{13}C]-GA present as the hydrate.[32]

Chart 1

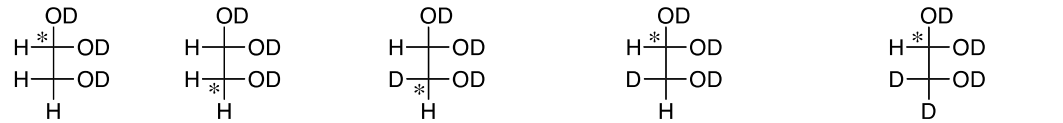

[1-^{13}C]-GA **[2-^{13}C]-GA** **[2-^{13}C, 2-^{2}H]-GA** **[1-^{13}C, 2-^{2}H]-GA** **[1-^{13}C, 2,2-di-^{2}H]-GA**

$$\ln f_S = - k_{obs} t \qquad (1)$$

$$(k_{cat} / K_m)_{obs} = \frac{k_{obs}}{(1 - f_{hyd})[TIM]} \qquad (2)$$

NMR Analyses of Protein Structure. Concentrated stock solutions of glycerol 3-phosphate for NMR experiments were prepared gravimetrically in the same buffer used for the enzyme solutions. The pH of this stock solution was adjusted to 6.6. All NMR samples were prepared in buffer containing 10 mM MES, 10 mM NaCl, 0.02% (w/v) NaN_3 and 7.5% D_2O at pH 6.6. Samples of *c*TIM were labeled with ^2H, ^{13}C, ^{15}N for chemical shift assignment or were uniformly (^2H, ^{15}N) labeled for ligand titration experiments. All NMR experiments were performed at a static magnetic field strength of 14.1 T on a Varian Inova spectrometer using a room temperature triple-resonance probe equipped with triple-axis gradients, with the exception that the HNCA experiments were performed at a static magnetic field strength of 21.2 T at the NMR Facilities Center at the University of Colorado. Experimental temperatures were calibrated using 100% methanol as a standard. NMR data were processed in NMRPipe [61] and analyzed using Sparky.[62] Two-dimensional ^1H-^{15}N NMR experiments for all protein samples were collected with identical parameters using spectral widths of 2400 x 8000 Hz and 256 x 2048 points in the t_1 and t_2 dimensions.

Three-dimensional backbone assignment experiments require uniformly enriched labeling of ^{15}N and ^{13}C. Resonance assignments for wild type cTIM were obtained from those determined by Dr. Jim Kempf in the Loria lab and deposited as BioMagResBank (BMRB) entry 15064.[45] Many resonances in mutant enzymes could be assigned by direct comparison with the wild type ^1H-^{15}N-correlation spectra. These assignments were confirmed and ambiguities were resolved using data from TROSY-based HN(CA)CB [63-65] and HNCA experiments.[66]

Binding of Glycerol-3-phosphate. Formation of the complex between G3P and wild

type *c*TIM was monitored at 25 °C in a series of TROSY-based ^{1}H-^{15}N-correlation experiments. Protein samples were uniformly labeled with ^{15}N and perdeuterated. Using known assignments the change in the chemical shift of well-resolved peaks, with increasing [G3P], was monitored until ligand saturation, when the chemical shifts were not affected by further ligand addition. Chemical shift changes were quantified by eq 3

$$\Delta\delta^{NH} = \sqrt{\frac{(H_{WT} - H_{mut})^2 + (N_{WT} - N_{mut})^2 / 25}{2}} \qquad (3)$$

in which H and N refer to the ^{1}H and ^{15}N residue specific chemical shifts for wildtype and mutant enzymes.[67]

RESULTS

The genes for the 167-PE-168 loop 6 replacement mutant (L6RM) and the 170-IGTG-173 loop deletion mutant (LDM) of *c*TIM were expressed using different *c*TIM-deficient strains of *E. coli.* The LDM was expressed from *E. coli* strain DF502 ($strep^{R}$, tpi^{-}, and his^{-}),[57] while the L6RM was expressed from the *tpi*A^{-} □DE3 lysogenic strain of *E. coli*, FB215471(DE3).[53,54] The latter strain shows more robust growth and gives the better yields of mutant enzyme.[53] The kinetic parameters determined here for the LDM-catalyzed isomerization of GAP at 25 °C are in agreement with the kinetic parameters reported by Knowles and coworkers reactions at 30 °C.[28]

Assignment of Backbone Amide Resonances from NMR. Three-dimensional TROSY-based triple-resonance NMR experiments were utilized to assign the backbone amide resonances in the L6RM. In addition to comparison with the assignments of wild type *c*TIM,[68] TROSY-based HN(CA)CB,[65] and HNCA [66] experiments were performed on the apo enzymes of L6RM *c*TIM. Because the backbone amide assignments are of primary interest, only the apo enzyme forms of the mutants were prepared for three-dimensional NMR assignment experiments with

triple isotope labeling. Backbone amide assignments for G3P-bound L6RM and wild type enzymes were obtained by performing a G3P titration experiment, during which ligand binding-induced chemical shift changes were monitored.

In total 94% and 92% of all non-proline backbone H,N resonances of the L6RM and the L6RM-G3P complex, respectively, were assigned. Assignments of the backbone amides were obtained for all of the non-proline residues in loop 6 of the L6RM (residues 166-176) and for all of the residues in loop 7 (residues 208-211), except for Gly-210. The signals for the backbone amides of six residues in the L6RM, that were assigned at the apo-enzyme, could not be identified for the enzyme-G3P complex, due to peak broadening, or to unresolved overlapping with neighboring peaks.

Mutation-induced changes in chemical shifts. A comparison of wild type and L6RM two-dimensional spectra are shown in Figure 2A. The chemical shift changes due to this mutation are quantified using equation 3 and shown in Figure 2B for each residue. The elevated values of δ^{NH} (> 0.2ppm) are mapped on the model for wild type *c*TIM shown in Figure 2C. Significant changes in the chemical shift for wild type *c*TIM were detected for the L6RM at residues Val161-Thr177, but the values of δ^{NH} for G171, G173, and K174 are slightly below 0.2 ppm. In loop 7, only V212 showed a $\delta^{NH} > 0.2$ ppm. The L6RM also showed significant δ^{NH} at helix E1 and at residues Gly128-Glu145 of helix E2 (Figure 2B).

Binding of glycerol-3-phosphate monitored by NMR. To investigate the effect of the L6RM on enzyme-ligand interactions, the binding of the substrate analog G3P to wild type *c*TIM and the L6RM on the amide chemical shifts were compared. Titrations at 298 K were monitored by collecting a two dimensional NMR spectrum at each titration point (Figure 3A and 3B). Intermediate exchange was detected at multiple residues in both wild type *c*TIM and the L6RM

as the peak intensities gradually diminish as the titration endpoint is approached. The differences in the patterns of the residue chemical shifts for this titration indicates substantial differences between the conformations of loop 6 for the wild type and L6RM enzymes. The final concentration of G3P in solutions of *c*TIM was increased to 90 mM and 290 mM, respectively, in NMR studies of wild type *c*TIM and the L6RM. Weak binding between G3P and wild type *c*TIM was observed, which is consistent with the value of K_i = 1.4 mM for G3P determined for TIM from yeast.[69] The titration also shows that the binding of L6RM to G3P is significantly weaker than in wild type *c*TIM.

Figure 3 illustrates the composite changes in chemical shift (δ^{NH}) upon G3P binding as a function of residue number in wild type *c*TIM (Figure 3C) and the L6RM (Figure 3D). The overall average of the values of δ^{NH} (eq 3) observed upon binding of G3P are 0.043 ± 0.050 ppm for wild type *c*TIM and 0.056 ± 0.040 ppm for the L6RM are not significantly different. However, site-specific differences in δ^{NH} induced by binding of G3P were noted for wild type *c*TIM and the L6RM. Dramatic responses to G3P binding are observed at multiple regions for the wild type enzyme, including loop 6 and loop 7, whereas in the L6RM enzyme the ligand-induced changes in the chemical shift at loop 6 are smaller; in particular, at residues in the N-terminal portion of the loop nearest the mutations (Figures 3E and 3F). Other residues at wild type *c*TIM, which show notable changes in chemical shift induced by the binding of G3P, include those in the vicinity of the active site such as N11, K12, H95, E97, G232, along with neighboring residues. In the L6RM mutant these same residues do not experience chemical shifts of similar magnitude indicating non wild type like ligand interactions at the active site.

Steady-State Kinetics. Figures 4A and 4B show the increase in v_i/[E] for the L6RM-catalyzed isomerization of GAP and DHAP, respectively, in solutions that contain 30 mM TEA

buffer, pH 7.5, I = 0.1 (NaCl) at 25 °C. The small downward curvature in these plots is consistent with either the formation of weak Michaelis complexes to substrate, or a small decrease in k_{cat}/K_m from a specific salt effect of replacing NaCl by the substrate dianion. There is no detectable decrease in $(k_{cat}/K_m)_{obs}$ for the L6RM-catalyzed isomerization of GAP in solutions that contain 30 mM TEA buffer, pH 7.5, I = 0.1 (NaCl) at 25 °C, as the concentration of the strong competitive inhibitor phosphoglycolate (PGA)[70] is increased to 10 mM (Figure S1, Supporting Information). This gives $K_i \geq 40$ mM (Table 1) for inhibition by PGA, if it is assumed that a 20% decrease in k_{cat}/K_m could have been detected for the reaction at 10 mM PGA. The values of k_{cat}/K_m for L6RM-catalyzed isomerization of DHAP and DGAP (Table 1) were determined from the slopes of strictly linear portions of the Michaelis-Menten plots shown in the insets to Figures 4A and 4B. The value of $k_{cat}/K_m = 470$ M^{-1} s^{-1} for L6RM-catalyzed isomerization of GAP (Table 1), and the assumption that PGA and GAP show a similar weak affinity for the L6RM (K_i, $K_m \geq 0.04$ M), gives a limit of $k_{cat} \geq 20$ s^{-1} for L6RM-catalyzed isomerization of GAP (Table 1).

Scheme 3

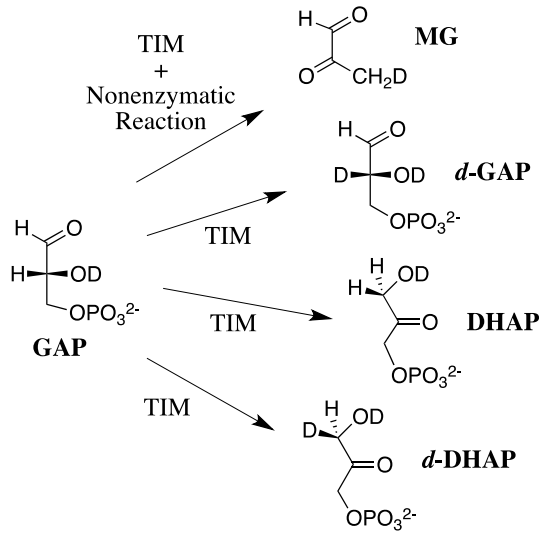

Mutant *c*TIM-Catalyzed Isomerization of GAP in D_2O. The mutant *c*TIM-catalyzed

reaction of GAP in D_2O was monitored by ^1H NMR spectroscopy, as described in previous work.[50] Three products form at the enzyme active site: DHAP, *d*-DHAP, and *d*-GAP; and, a fourth product, methylglyoxal, may form by nonenzymatic and enzyme-catalyzed reactions (Scheme 3).[31] The yield of each product, $(f_P)_{obs}$ was calculated from the normalized ^1H NMR peak area for a single proton for the particular product (A_P, eq 4) and the sum of the peak areas of single protons for all of the reaction products, as described in previous work.[50] The fraction of GAP remaining at a given reaction time (f_{GAP}) was calculated as the ratio of the normalized ^1H NMR peak area of a single proton of the remaining GAP, and the sum of the normalized ^1H NMR peak areas of single protons for GAP and for each reaction product.[50]

$$(f_P)_{obs} = \frac{A_P}{A_{DHAP} + A_{d\text{-}DHAP} + A_{d\text{-}GAP} + A_{MG}} \qquad (4)$$

$$(f_{MG})_N = \frac{k_N}{k_{obs}} \qquad (5)$$

$$(f_{MG})_E = (f_{MG})_{obs} - (f_{MG})_N \qquad (6)$$

Figure 5A shows the decrease in f_{GAP} with time during the reaction of 10 mM GAP catalyzed by 0.4 μM L6RM *c*TIM in D_2O buffered by 10 mM imidazole (70% free base), I = 0.1 (NaCl) at pD 7.9 and 25 °C. The fit of the data from Figure 5A to a single exponential decay gave $k_{obs} = 2.7 \times 10^{-4}$ s^{-1} for the disappearance of GAP. Figure 5B shows the change with time in the fractional product yields $(f_P)_{obs}$ (eq 4) for DHAP, *d*-DHAP, *d*-GAP during a 150 min L6RM-catalyzed reaction of GAP. The yields of DHAP, *d*-DHAP, and *d*-GAP, determined by extrapolation of the product yields (Figure 5B) to zero reaction time, are reported in Table 2. A 4% yield of MG was also observed. Combining k_N = 1.7 x 10^{-5} s^{-1} determined for the nonenzymatic elimination reaction of GAP in D_2O at pD 7.9 (10 mM imidazole), 25 ˚C and I = 0.15 (NaCl),[27] and k_{obsd} = 2.7 x 10^{-4} s^{-1} determined from the fit of data in Figure 5A, gives a

theoretical yield of $(f_{MG})_N = 0.06$ (eq 5) if MG forms exclusively by nonenzymatic elimination in the presence of 0.4 μM L6RM *c*TIM in D_2O. This is not significantly different from $(f_{MG})_{obs}$ = 0.04 (Table 2). We conclude that MG forms mainly or entirely by a nonenzymatic reaction.

Figure 5C shows the decrease in f_{GAP} with time during the reaction of 10 mM GAP catalyzed by 7 μM LDM *c*TIM in D_2O buffered by 10 mM imidazole (70% free base), $I = 0.1$ (NaCl) at pD 7.9 and 25 °C. The fit of the data from Figure 5C to a single exponential decay gave $k_{obs} = 7.5 \times 10^{-5}$ s^{-1} for the disappearance of GAP. Figure 5D shows the change with time in the fractional product yields $(f_P)_{obs}$ (eq 4) for DHAP, *d*-DHAP, *d*-GAP and MG during a 360 min reaction time. The yields of DHAP, *d*-DHAP, *d*-GAP, and MG determined by extrapolation of the product yields (Figure 5D) to zero reaction time, are reported in Table 2. Table 2 also reports the normalized yield of products from proton transfer reactions at the enzyme active site, DHAP, *d*-DHAP, *d*-GAP, calculated using eq. 7 – 9.

$$(f_{d\text{-}GAP})_E = \frac{f_{d\text{-}GAP}}{f_{d\text{-}GAP} + f_{DHAP} + f_{d\text{-}DHAP}} \quad (7)$$

$$(f_{DHAP})_E = \frac{f_{DHAP}}{f_{d\text{-}GAP} + f_{DHAP} + f_{d\text{-}DHAP}} \quad (8)$$

$$(f_{d\text{-}DHAP})_E = \frac{f_{d\text{-}DHAP}}{f_{d\text{-}GAP} + f_{DHAP} + f_{d\text{-}DHAP}} \quad (9)$$

Combining $k_{obs} = 7.5 \times 10^{-5}$ s^{-1} for the reaction of GAP in the presence of 7 µM of LDM *c*TIM and $k_N = 1.7 \times 10^{-5}$ s^{-1} gives $(f_{MG})_N = 0.23$ (eq 5) for the fractional yield of methylglyoxal from the nonenzymatic elimination reaction (Table 2). The observed yield of MG, $(f_{MG})_{obs}$ = 0.75, so that the yield from the LDM-catalyzed reaction is $(f_{MG})_E = 0.52$ (eq 6). By comparison, Knowles and coworkers reported 85% and 15% yields of MG and DHAP, respectively, from the LDM-catalyzed reaction of GAP in H_2O.[28]

Mutant *c*TIM-Catalyzed Reactions of [1-^{13}C]-GA in D_2O. The following reactions of solutions of 20 mM [1-^{13}C]-GA were monitored by ^{1}H NMR spectroscopy: (a) The reaction catalyzed by 0.32 mM LDM *c*TIM in 20 mM imidazole buffer, I = 0.1 (NaCl) at 25 °C was monitored for 140 h, during which time the loss of 60% of total [1-^{13}C]-GA was observed. (b) The reaction catalyzed by 0.32 mM LDM *c*TIM in the presence of 40 mM phosphite (50% dianion) in 6 mM imidazole buffer, I = 0.1 (NaCl) at 25 °C was monitored for 140 h, during which time the loss of 80% of total [1-^{13}C]-GA was observed. (c) The reaction catalyzed by 0.39 mM L6RM *c*TIM in 20 mM imidazole buffer, I = 0.1 (NaCl) at 25 °C was monitored for 90 h, during which time the loss of 43% total [1-^{13}C]-GA was observed. (d) The reaction of [1-^{13}C]-GA catalyzed by 0.23 mM L6RM *c*TIM in the presence of 40 mM phosphite (50% dianion) in 6 mM imidazole buffer, I = 0.1 (NaCl) at 25 °C was monitored for 30 h, during which time the loss of 30% of total [1-^{13}C]-GA was observed. The observed first-order rate constant, k_{obs} (s^{-1}), for the disappearance of [1-^{13}C]-GA and the observed second-order rate constant $(k_{cat}/K_m)_{obs}$, determined as described in the Experimental Section, are reported in Table 3.

Scheme 4

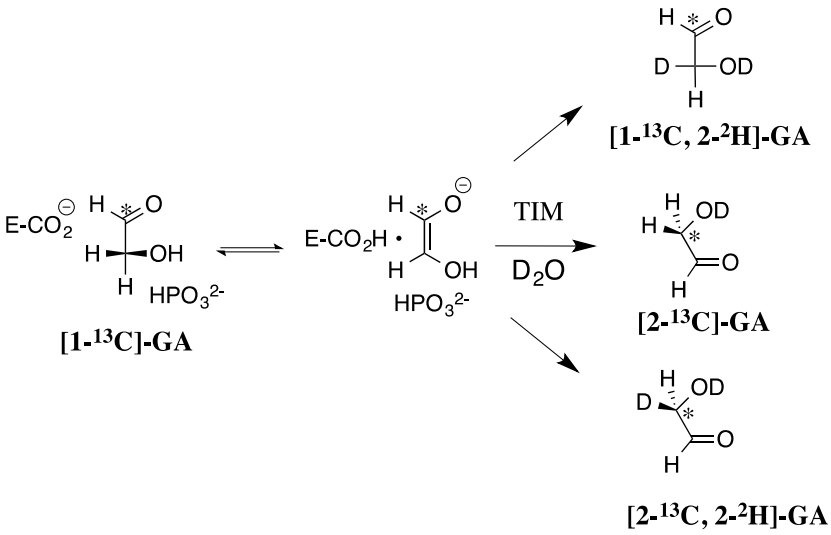

Chart 1 shows the four products of the TIM-catalyzed reaction of [1-^{13}C]-GA:

[2-^{13}C]-GA; [2-^{13}C, 2-^{2}H]-GA, [1-^{13}C, 2-^{2}H]-GA and [1-^{13}C, 2,2-di-^{2}H]-GA.[33,53,71-73] The dideuterated product [1-^{13}C, 2,2-di-^{2}H]-GA forms in a nonspecific protein-catalyzed reaction.[27,33,74] Scheme 4 shows the isomerization products [2-^{13}C]-GA and [2-^{13}C, 2-^{2}H]-GA, which form at the active site of TIM (Scheme 4) and [1-^{13}C, 2-^{2}H]-GA, which may form either at the enzyme active site or in a nonspecific protein-catalyzed reaction.[27,33,74] The major product of the LDM-catalyzed reaction, [1-^{13}C, 2,2-di-^{2}H]-GA, forms in a yield of 39% and 34%, respectively, for the reactions in the absence and presence of 0.020 M HP_i. No [2-^{13}C]-GA or [2-^{13}C, 2-^{2}H]-GA was detected from the LDM-catalyzed reactions, but [1-^{13}C, 2-^{2}H]-GA forms in 10% and 15% yields, respectively, for the reactions in the absence and presence of the dianion activator. The sum of the *observed* product yields from these slow, mainly protein-catalyzed reactions is less than 100%.[33,75,76] The other products, from the slow nonenzymatic reactions of glycolaldehyde, have not been identified.[32]

Scheme 5

$$E \underset{K_{GA}}{\overset{\pm GA}{\rightleftharpoons}} E{\bullet}GA \underset{K_{HPi}}{\overset{\pm HPO_3^{2-}}{\rightleftharpoons}} E{\bullet}GA{\bullet}HPO_3^{2-} \xrightarrow{k_{cat}} E + P$$

$$\frac{k_{cat}}{K_{HPi}K_{GA}} = \left[\frac{(k_{cat}/K_m)_{obs}}{[HPO_3^{2-}]}\right] \sum (f_P)_E \qquad (10)$$

The major product of the L6RM-catalyzed reactions of [1-^{13}C]-GA in the absence (28 % yield) and presence of 0.020 M HP_i (34% yield) is [1-^{13}C, 2,2-di-^{2}H]-GA from a nonspecific protein-catalyzed reaction.[74] In the presence of 0.020 M HP_i , small 0.2% and 2% yields, respectively of the products of isomerization at the active site, [2-^{13}C]-GA and [2-^{13}C, 2-^{2}H]-GA, were observed, along with a 10% yield of [1-^{13}C, 2-^{2}H]-GA. In the absence of HP_i, no [2-^{13}C]-

GA and [2-^{13}C, 2-^{2}H]-GA were detected, and the yield of [1-^{13}C, 2-^{2}H]-GA was 7%. In both cases the yield of [1-^{13}C, 2-^{2}H]-GA is similar to that for the LDM-catalyzed reactions (above), for which *no products* of isomerization at the enzyme active site are observed. This suggests that [1-^{13}C, 2-^{2}H]-GA forms *mainly* by non-specific protein catalyzed reactions of the LDM and L6RM. An *approximate* value of 0.5 M^{-2} s^{-1} for ($k_{cat}/K_{HPi}K_{GA}$) was calculated for the LR6M-catalyzed reaction (Scheme 5), using eq 10, $(k_{cat}/K_m)_{obs}$ = 0.25 M^{-1} s^{-1} (Table 3), [HPO_3^{2-}] = 0.020 M and the *approximate* product yield of $\Sigma(f_P)_E \approx 0.04$. This yield was estimated by assuming equal 0.02 fractional yields of deuterium labeled products [1-^{13}C, 2-^{2}H]-GA and [2-^{13}C, 2-^{2}H]-GA from reactions of [1-^{13}C]-GA at the active site of the L6RM of TIM

X-Ray Crystal Structure for the L6RM. Solutions of the L6RM were screened robotically against 288 precipitant conditions from the Hampton Research's HT screens. Numerous precipitant conditions generated crystals. Ultimately, a solution containing PEG 3350 and Tris pH 8.5 produced L6RM crystals that diffracted to 1.3 Å. Through utilization of molecular replacement initial phase information was obtained, which yielded the structure of the L6RM as a dimer in a C2 space group. Data refinement and collection statistics for the L6RM crystal structure are presented in Table S1 of the Supporting Information.

The overall secondary and quaternary X-ray structure of L6RM is a TIM barrel. Gaps in the electron density in the region of loop 6 are observed for both subunits A and B, with subunit A showing the smaller gap, which runs from residues 173 – 175 (Figure S2, Supporting Information). A close inspection of the region-containing loop 6 reveals several important differences from the structure for wild type *c*TIM and of several other loop 6 mutants (1SU5, 1SW0, 1SW3, 1SW7).[77] Figure 6A shows that W168 of wild type cTIM is directed toward the protein core by a cation-pi interaction[78] with the side chain of R134; and, Figure 6B shows that

formation of a complex to the intermediate analog phosphoglycolohydroxamate (PGH) induces a conformational change, which replaces the cation-pi interaction by a hydrogen bond between the indole -NH and the carboxylate side chain of E129 (Figure 6B). By contrast, the better-defined structure for subunit A of the L6RM shows the carboxylate side chain of E168 displaced toward solution, compared with wild type *c*TIM, probably to relieve destabilizing interactions with the side chain of E129 (Figure 6C). The structure for loop 6 in TIM from eukaryotes and bacteria is similar to that for archeal TIM,[79-81] because the equivalent N-terminal hinge residues (W168 or E147) are stabilized by functionally equivalent interactions with the protein core. This is shown by the X-ray crystal structure of TIM from *Pyrococcus woesei* (*Pw*TIM) liganded to 3-phosphonopropanoic acid, where the glutamate side chain of the 145-PPE-147 hinge interacts with the protein core through a salt bridge to the side chain of K159 (Figure 6D).

DISCUSSION

Sun and Sampson have prepared a library of 8000 mutants of the N-terminal hinge of *c*TIM from chicken muscle [166-XXX-168].[43,44,82] Only 3% of the library members complement a DF502 TIM-deficient strain of E. *coli* and show ≈ 70% of the wild type enzyme activity.[44] Several non-complementing members of this library were characterized, including the glycine rich 166-GGG-168 mutant, which showed a 130-fold falloff in k_{cat}/K_m.[44] These glycine mutations were proposed to result in an increase in the number of protein conformations for the loop-open form of TIM. This corresponds to the entropic stabilization of the open enzyme compared with the active rigid closed form of TIM, which results in a significant entropic price for *ordering* the flexible loop at the closed enzyme.[45,46]

The contribution of interactions between loop 6 and the substrate phosphodianion to

catalysis by TIM were examined in this work by eliminating these interactions in the I170-G173 LDM,[28] and by modifying these interactions in the L6RM. The LDM and L6RM result in large 800,000 and 23,000-fold decreases, respectively, in k_{cat}/K_m for isomerization of GAP. Each mutation results in a decrease in the affinity of substrates and intermediate analogs PGA or PGH for *c*TIM (Table 1), but the ligands bind significantly *more tightly* to the LDM, where there can be no stabilization of ligand by interactions with loop 6, compared with the L6RM, where the loop-ligand interactions have been modified (Table 1). This shows that complexes to the L6RM are destabilized by the interaction between the ligand and modified loop 6.

X-Ray Crystallographic and NMR Structural Studies. The X-ray crystallographic and NMR structural data were obtained for proteins in solutions that contain the same buffer. The crystal structure of the unliganded L6RM shows that this substitution introduces a kink into loop 6, which results in a large displacement of the carboxylate side chain of Glu-168 from the position of the tryptophan side chain of W168 for the wild type enzyme (Figure 6C). There is a smaller movement in the position of the side-chains for the tip residues and a good overlap of the residues at the C-terminal hinge, and in the positions of the catalytic side chains for H95 and E165. The L6RM leads to significant changes in the chemical shifts for nuclei at loop 6, and elsewhere in the protein (Figure 2B). An NMR titration shows that G3P binds with a higher affinity to wild type cTIM compared with the L6RM. The binding of G3P induces significant changes in the chemical shifts for multiple nuclei in the regions of loop 6 and loop 7 of wild type *c*TIM, and nuclei associated with residues 10-13, 94 and 95 (Figure 3C), but substantially smaller changes in the chemical shifts for the corresponding nuclei at the L6RM (Figure 3D). This shows that there are substantial differences in the enzyme conformational change associated with the binding of G3P to wild type *c*TIM and the L6RM.

The LDM provides a benchmark for the catalytic properties of TIM for a case where there is minimal enzyme activation by loop closure over the substrate phosphodianion. The differences between the kinetic parameters and products for the benchmark LDM- and L6RM-catalyzed reactions provides strong evidence that the mutant loop 6 of the L6RM plays an activating role by closing over the ligand phosphodianion at the transition state for the TIM-catalyzed isomerization reaction

(1) The > 700-fold larger value of k_{cat} for the L6RM (> 20 s^{-1}) compared with the LDM-catalyzed (0.03 s^{-1}) isomerization of GAP (Table 1) shows that the transition state for the former reaction is stabilized by interactions with gripper loop residues.

(2) Good yields for the elimination reaction product methylglyoxal are obtained from the LDM-catalyzed reaction of GAP, due to the loss of interactions between the tip residues of loop 6 and the enediolate intermediate, which stabilize the intermediate towards elimination of inorganic phosphate.[28,31] By contrast, no products of an L6RM-catalyzed elimination reaction are observed. This provides strong evidence that there is a strong stabilization of the bound intermediate towards elimination of inorganic phosphate by interactions with loop 6.

Scheme 6

$$E_O \overset{K_d}{\rightleftharpoons} E_O{\bullet}GAP \overset{K_c}{\rightleftharpoons} E_C{\bullet}GAP \xrightarrow{k_{cat}} E + DHAP$$

We therefore propose that GAP and DHAP form Michaelis complexes to the L6RM, that are destabilized by interactions with the twisted loop, and that these complexes isomerize to the active loop-closed enzyme, with loop 6 positioned similar to that for wild type *c*TIM. Interactions between TIM and the appropriate spectator dianion, such as the phosphodianion of GAP or HP_i, lock the enzyme into a catalytically active form that is otherwise present at low concentrations.[16,17,53,83,84] This is shown in Scheme 6, where GAP binds to form an initial

nonproductive complex to TIM and the conformational change to form the active closed enzyme is favorable ($K_C >> 1$, Scheme 6). Our results provide evidence that loop closure at the Michaelis complex to the L6RM is unfavorable ($K_C << 1$, Scheme 6), because this creates destabilizing electrostatic stress between the carboxylate side chains of E168 and E129 (Figure 6B). The weak ligand binding to the L6RM shows that there is a large energetic price for removing the kink in loop 6, as this loop closes over the ligand dianion. Consequently, a large fraction of the intrinsic ligand binding energy is utilized to drive the enzyme conformational change, so that little binding energy is available to stabilize the Michaelis complex. These results are consistent with a malleable protein structure for TIM where the effect of mutations such as the L6RM, which distort the protein structure, may be overcome by utilization of the phosphodianion binding energy available to *mold* the enzyme into the catalytically active loop-closed conformation.

Partitioning of the Reaction Intermediate. Table 2 reports the products of the partitioning of the enediolate intermediate of the reaction of *h*-GAP in D_2O. These product yields define the macroscopic rate constant ratio $(k_{C1})_H/k_{ex}$ (eq 11) for partitioning of the intermediate labeled with –H at the carboxylic acid side chain of Glu-165, between exchange of the –H for –D from solvent to give deuterium labeled products, and transfer of –H to C-1 of the intermediate to form DHAP; and, $(k_{C1})_D/(k_{C2})_D$ (eq 12) for partitioning of the enediolate intermediate labeled with –D at the carboxylic acid side chain of Glu-165 between hydron transfer to C-1 and C-2 to form *d*-DHAP and *d*-GAP, respectively.

$$\frac{(k_{C1})_H}{k_{ex}} = \frac{[\text{DHAP}]}{[d\text{-DHAP}] + [d\text{-GAP}]} \qquad (11)$$

$$\frac{(k_{C1})_D}{(k_{C2})_D} = \frac{[d\text{-DHAP}]}{[d\text{-GAP}]} \qquad (12)$$

The rate constant ratios $(k_{C1})_H/k_{ex} = 0.04$ or 0.05 and $(k_{C1})_D/(k_{C2})_D = 0.09$ or 0.10

determined for partitioning of the enediolate phosphate intermediates of the LDM- and the L6RM-catalyzed reactions, respectively, of GAP in D_2O are remarkably similar to one another, but different from the ratios of $(k_{C1})_H/k_{ex} = 0.96$ and $(k_{C1})_H/k_{ex} = 1.48$ determined for wild type *c*TIM (Table 2).[50] We conclude that these mutations result in a decrease in the velocity for formation of *h*-DHAP relative to rate of exchange of –H labeled TIM with deuterium from solvent, and in the rate of formation of *d*-DHAP relative to the rate of formation *d*-DGAP (Figure 7). Formation of both *h*-DHAP and *d*-DHAP requires hydron migration from O-2 to O-1 of the enediolate phosphate generated by deprotonation of GAP that is facilitated by the imidazole side chain of His-95 (Figure 7).[11] Our results suggest that hydron migration between O-2 and O-1 is relatively fast and supports efficient wild type *c*TIM-catalyzed isomerization; but, that this migration is impaired at the LDM and L6RM, so that internal return of the O-2 protonated enediolate phosphate to *h*-GAP and *d*-GAP is favored. The result is that a larger fraction of substrate deprotonation steps are nonproductive and result in either "hidden" internal return to regenerate *h*-GAP or the formation of *d*-GAP. The fast washout of hydrogen from the active sites of the LDM and L6RM, to give a 95 – 96% yield of deuterium labeled product may also reflect an increase in the accessibility of the active site to bulk solvent.

Dianion Activation of *c*TIM Catalyzed Reactions of [1-^{13}C]-GA. The major products of the LDM- and L6RM-catalyzed reactions are [1-^{13}C, 2,2-di-^{2}H]-GA (30 %) from a nonspecific protein catalyzed reaction, [1-^{13}C, 2-^{2}H]-GA (10 %) which may form either from an exchange reaction at the active site of TIM, or from a nonspecific protein catalyzed reaction.[33,75,76] No [2-^{13}C]-GA or [2-^{13}C, 2-^{2}H]-GA are observed from the LDM-catalyzed reactions of [1-^{13}C]-GA in the absence or the presence of 20 mM HP_i; but, the L6RM *c*TIM-catalyzed reaction of [1-^{13}C]-GA gives 0.2% and 2% yields, respectively, of [2-^{13}C]-GA, [2-^{13}C,

2-^{2}H]-GA from formal isomerization reactions at the enzyme active site. We conclude that the L6RM shows barely detectable activation by HP_i. We estimate a value of $k_{cat}/K_{GA}K_{HPi} \approx 0.5\ M^{-2}\ s^{-1}$ (eq 10 for Scheme 5) for the reaction activated by 20 mM phosphite dianion (Results section), but that this rate constant is not significantly different from 0 for the LDM.

Figure 8 shows the recently reported linear free energy relationship, with slope 1.04 ± 0.03, between values of $\log(k_{cat}/K_m)_{GAP}$ for wild type and mutant TIM-catalyzed reactions of (*R*)-GAP and $\log(k_{cat}/K_{HPi}K_{GA})$ for reactions of the substrate pieces glycolaldehyde and HP_i (Scheme 5).[84] The horizontal dotted line is drawn for the estimated limiting rate constant of $k_{cat}/K_{HPi}K_{GA} = 0.25\ M^{-2}\ s^{-1}$ for activation by 0.020 M HP_i, and assuming $(k_{cat}/K_m)_{obs} = 0.25\ M^{-1}\ s^{-1}$ (Table 3) and that the yield of the products of the specific TIM-catalyzed reactions is $\Sigma(f_P)_E < 0.02$ (eq 10), which would be difficult or impossible to detect by our methods. This limiting rate constant is approached for mutant forms of TIM as $(k_{cat}/K_m)_{GAP}$ approaches $10^4\ M^{-1}\ s^{-1}$. By comparison, values of $(k_{cat}/K_m)_{GAP} = 470$ and $14\ M^{-1}\ s^{-1}$ were determined, respectively, for the L6RM and the LDM. The value of $k_{cat}/K_{HPi}K_{GA} = 0.5\ M^{-2}\ s^{-1}$ estimated for the L6RM shows a positive deviation from the linear correlation in Figure 8, and a similar positive deviation has been reported for the loop 7 replacement mutant of *c*TIM.[53,84] We conclude that the failure to observe activation of the LDM by phosphite dianion is as expected for the 800,000-fold smaller value of $(k_{cat}/K_m)_{GAP}$ for the LDM, compared with wild type *c*TIM-catalyzed reactions. These results are consistent with the conclusion that a functioning loop 6 is required to observe dianion activation of TIM for catalysis of deprotonation of bound substrate, but they do not definitively exclude the possibility of weak dianion activation of reactions catalyzed by the LDM.

Conclusions. The results reported here are consistent with the requirement that TIM undergo an energetically uphill change in conformation from an inactive open conformation to

an active closed form, which is driven by the intrinsic phosphodianion binding energy.[16,17,33,53,71] Catalysis by the L6RM provides a remarkable example of the *plasticity* of the structure of *c*TIM. We find that the severe distortion in structure of the unliganded wildtype enzyme (Figure 6C) may be overcome by the utilization of phosphodianion binding energy to mold *c*TIM into the catalytically active closed form. The observed binding of the substrate dianion to the L6RM is consequently much weaker than for wild type TIM. By contrast, there is compelling evidence that the L232A mutation of TIM from *Trypanosoma brucei* reduces the barrier for the phosphodianion driven conformational change.[71,73] The result of this reduced barrier to formation of the catalytically active enzyme is that a larger fraction of the total dianion binding energy is expressed at Michaelis complexes to GAP, DHAP and HP_i.[71,73]

Acknowledgement. The authors thank the supporting member institutions of SER-CAT 22-BM at the Advanced Photon Source, Argonne National Laboratory, these institutions can be found at www.ser-cat.org/members.html and http://ls-cat.org respectively. JPR thanks Professor Nicole Sampson for her guidance in the preparation of the loop deletion mutant.

SUPPORTING INFORMATION

TableS1: Statistics from X-ray data collection and refinement for the X-ray crystal structure of the L6RM. Figure S1: Dependence of the apparent second-order rate constant $(k_{cat}/K_m)_{app}$ for the isomerization of GAP, catalyzed by the L6RM of *c*TIM, on the concentration of PGA. Figure S2: A figure which shows the electron density in the region of loop 6 for subunit A of the L6RM of cTIM. This material is available free of charge via the Internet at http://pubs.acs.org.

REFERENCES

1. Fothergill-Gilmore, L. A. (1986) The evolution of the glycolytic pathway. *Trends Biochem. Sci. 11*, 47-51.
2. Knowles, J. R., and Albery, W. J. (1977) Perfection in enzyme catalysis: the energetics of triosephosphate isomerase. *Acc. Chem. Res. 10*, 105-111.
3. Knowles, J. R. (1991) To build an enzyme. *Philos. Trans. R. Soc. London, Ser. B 332*, 115-121.
4. Waley, S. G., Miller, J. C., Rose, I. A., and O'Connell, E. L. (1970) Identification of site in triose phosphate isomerase labeled by glycidol phosphate. *Nature (London) 227*, 181.
5. De la Mare, S., Coulson, A. F. W., Knowles, J. R., Priddle, J. D., and Offord, R. E. (1972) Active-site labeling of triose phosphate isomerase. Reaction of bromohydroxyacetone phosphate with a unique glutamic acid residue and the migration of the label to tyrosine. *Biochem. J. 129*, 321-331.
6. Straus, D., Raines, R., Kawashima, E., Knowles, J. R., and Gilbert, W. (1985) Active site of triosephosphate isomerase: in vitro mutagenesis and characterization of an altered enzyme. *Proc. Natl. Acad. Sci. 82*, 2272-2276.
7. Zhang, Z., Komives, E. A., Sugio, S., Blacklow, S. C., Narayana, N., Xuong, N. H., Stock, A. M., Petsko, G. A., and Ringe, D. (1999) The Role of Water in the Catalytic Efficiency of Triosephosphate Isomerase. *Biochemistry 38*, 4389-4397.
8. Malabanan, M. M., Nitsch-Velasquez, L., Amyes, T. L., and Richard, J. P. (2013) Magnitude and origin of the enhanced basicity of the catalytic glutamate of triosephosphate isomerase. *J. Am. Chem. Soc. 135*, 5978-5981.

9. Lodi, P. J., and Knowles, J. R. (1991) Neutral imidazole is the electrophile in the reaction catalyzed by triosephosphate isomerase: structural origins and catalytic implications. *Biochemistry 30*, 6948-6956.

10. Komives, E. A., Chang, L. C., Lolis, E., Tilton, R. F., Petsko, G. A., and Knowles, J. R. (1991) Electrophilic catalysis in triosephosphate isomerase: the role of histidine-95. *Biochemistry 30*, 3011-3019.

11. Nickbarg, E. B., Davenport, R. C., Petsko, G. A., and Knowles, J. R. (1988) Triosephosphate isomerase: removal of a putatively electrophilic histidine residue results in a subtle change in catalytic mechanism. *Biochemistry 27*, 5948-5960.

12. Wise, E., Yew, W. S., Babbitt, P. C., Gerlt, J. A., and Rayment, I. (2002) Homologous $(\beta/\alpha)_8$-Barrel Enzymes That Catalyze Unrelated Reactions: Orotidine 5'-Monophosphate Decarboxylase and 3-Keto-L-Gulonate 6-Phosphate Decarboxylase. *Biochemistry 41*, 3861-3869.

13. Nagano, N., Orengo, C. A., and Thornton, J. M. (2002) One fold with many functions: The evolutionary relationships between TIM barrel families based on their sequences, structures and functions. *J. Mol. Biol. 321*, 741-765.

14. Wierenga, R. K. (2001) The TIM-barrel fold: a versatile framework for efficient enzymes. *FEBS Lett. 492*, 193-198.

15. Malabanan, M. M., Amyes, T. L., and Richard, J. P. (2010) A role for flexible loops in enzyme catalysis. *Cur. Opin. Struct. Biol. 20*, 702-710.

16. Richard, J. P., Amyes, T. L., Goryanova, B., and Zhai, X. (2014) Enzyme architecture: on the importance of being in a protein cage. *Cur. Opin. Chem. Biol. 21*, 1-10.

17. Richard, J. P. (2012) A Paradigm for Enzyme-Catalyzed Proton Transfer at Carbon: Triosephosphate Isomerase. *Biochemistry 51*, 2652-2661.

18. Amyes, T. L., and Richard, J. P. (2013) Specificity in Transition State Binding: The Pauling Model Revisited. *Biochemistry 52*, 2021-2035.

19. Amyes, T. L., Richard, J. P., and Tait, J. J. (2005) Activation of orotidine 5'-monophosphate decarboxylase by phosphite dianion: The whole substrate is the sum of two parts. *J. Am. Chem. Soc. 127*, 15708-15709.

20. Goryanova, B., Amyes, T. L., Gerlt, J. A., and Richard, J. P. (2011) OMP Decarboxylase: Phosphodianion Binding Energy Is Used To Stabilize a Vinyl Carbanion Intermediate. *J. Am. Chem. Soc. 133*, 6545-6548.

21. Tsang, W.-Y., Amyes, T. L., and Richard, J. P. (2008) A substrate in pieces: Allosteric activation of glycerol 3-phosphate dehydrogenase (NAD^+) by phosphite dianion. *Biochemistry 47*, 4575-4582.

22. Ray, W. J., Jr., Long, J. W., and Owens, J. D. (1976) An analysis of the substrate-induced rate effect in the phosphoglucomutase system. *Biochemistry 15*, 4006-4017.

23. Kholodar, S. A., and Murkin, A. S. (2013) DXP Reductoisomerase: Reaction of the Substrate in Pieces Reveals a Catalytic Role for the Nonreacting Phosphodianion Group. *Biochemistry 52*, 2302-2308.

24. Wierenga, R. K. (2010) Triosephosphate isomerase: a highly evolved biocatalyst. *Cell. Mol. Life Sci. 67*, 3961-3982.

25. Samanta, M., Murthy, M. R. N., Balaram, H., and Balaram, P. (2011) Revisiting the Mechanism of the Triosephosphate Isomerase Reaction: The Role of the Fully Conserved Glutamic Acid 97 Residue. *Chembiochem 12*, 1886-1895.

26. Go, M. K., Amyes, T. L., and Richard, J. P. (2010) Rescue of K12G mutant TIM by NH_4^+ and alkylammonium cations: The reaction of an enzyme in pieces. *J. Am. Chem. Soc. 132*, 13525-13532.

27. Go, M. K., Koudelka, A., Amyes, T. L., and Richard, J. P. (2010) Role of Lys-12 in Catalysis by Triosephosphate Isomerase: A Two-Part Substrate Approach. *Biochemistry 49*, 5377-5389.

28. Pompliano, D. L., Peyman, A., and Knowles, J. R. (1990) Stabilization of a reaction intermediate as a catalytic device: definition of the functional role of the flexible loop in triosephosphate isomerase. *Biochemistry 29*, 3186-3194.

29. Richard, J. P. (1993) Mechanism for the formation of methygloxal from triosephosphates. *Biochem. Soc. Trans. 21*, 549-553.

30. Richard, J. P. (1991) Kinetic-parameters for the elimination reaction catalyzed by triosephosphate isomerase and an estimation of the reactions physiological significance. *Biochemistry 30*, 4581-4585.

31. Richard, J. P. (1984) Acid-base catalysis of the elimination and isomerization reactions of triose phosphates. *J. Am. Chem. Soc. 106*, 4926-4936.

32. Amyes, T. L., and Richard, J. P. (2007) Enzymatic catalysis of proton transfer at carbon: Activation of triosephosphate isomerase by phosphite dianion. *Biochemistry 46*, 5841-5854.

33. Go, M. K., Amyes, T. L., and Richard, J. P. (2009) Hydron Transfer Catalyzed by Triosephosphate Isomerase. Products of the Direct and Phosphite-Activated Isomerization of [1-^{13}C]-Glycolaldehyde in D_2O. *Biochemistry 48*, 5769-5778.

34. Goryanova, B., Spong, K., Amyes, T. L., and Richard, J. P. (2013) Catalysis by Orotidine 5'-Monophosphate Decarboxylase: Effect of 5-Fluoro and 4'-Substituents on the Decarboxylation of Two-Part Substrates. *Biochemistry 52*, 537-546.

35. Amyes, T. L., Ming, S. A., Goldman, L. M., Wood, B. M., Desai, B. J., Gerlt, J. A., and Richard, J. P. (2012) Orotidine 5'-monophosphate decarboxylase: Transition state stabilization from remote protein-phosphodianion interactions. *Biochemistry 51*, 4630-4632.

36. Joseph, D., Petsko, G. A., and Karplus, M. (1990) Anatomy of a conformational change: hinged "lid" motion of the triosephosphate isomerase loop. *Science 249*, 1425-1428.

37. Xu, Y., Lorieau, J., and McDermott, A. E. (2010) Triosephosphate isomerase: ^{15}N and ^{13}C chemical shift assignments and conformational change upon ligand binding by magic-angle spinning solid-state NMR spectroscopy. *J. Mol. Biol. 397*, 233-248.

38. Rozovsky, S., and McDermott, A. E. (2001) The time scale of the catalytic loop motion in triosephosphate isomerase. *J. Mol. Biol. 310*, 259-270.

39. Rozovsky, S., Jogl, G., Tong, L., and McDermott, A. E. (2001) Solution-state NMR investigations of triosephosphate isomerase active site loop motion: Ligand release in relation to active site loop dynamics. *J. Mol. Biol. 310*, 271-280.

40. Massi, F., Wang, C., and Palmer, A. G., III. (2006) Solution NMR and computer simulation studies of active site loop motion in triosephosphate isomerase. *Biochemistry 45*, 10787-10794.

41. Berlow, R. B., Igumenova, T. I., and Loria, J. P. (2007) Value of a Hydrogen Bond in Triosephosphate Isomerase Loop Motion. *Biochemistry 46*, 6001-6010.

42. Desamero, R., Rozovsky, S., Zhadin, N., McDermott, A., and Callender, R. (2003) Active site loop motion in triosephosphate isomerase: T-Jump relaxation spectroscopy of thermal activation. *Biochemistry 42*, 2941-2951.

43. Sun, J., and Sampson, N. S. (1999) Understanding protein lids: kinetic analysis of active hinge mutants in triosephosphate isomerase. *Biochemistry 38*, 11474-11481.

44. Sun, J., and Sampson, N. S. (1998) Determination of the amino acid requirements for a protein hinge in triosephosphate isomerase. *Protein Sci. 7*, 1495-1505.

45. Kempf, J. G., Jung, J.-y., Ragain, C., Sampson, N. S., and Loria, J. P. (2007) Dynamic requirements for a functional protein hinge. *J. Mol. Biol. 368*, 131-149.

46. Xiang, J., Jung, J.-y., and Sampson, N. S. (2004) Entropy effects on protein hinges: The reaction catalyzed by triosephosphate isomerase. *Biochemistry 43*, 11436-11445.

47. Kursula, I., Salin, M., Sun, J., Norledge, B. V., Haapalainen, A. M., Sampson, N. S., and Wierenga, R. K. (2004) Understanding protein lids: structural analysis of active hinge mutants in triosephosphate isomerase. *Protein Eng., Des. Sel. 17*, 375-382.

48. O'Donoghue, A. C., Amyes, T. L., and Richard, J. P. (2008) Slow proton transfer from the hydrogen-labelled carboxylic acid side chain (Glu-165) of triosephosphate isomerase to imidazole buffer in D_2O. *Org. Biomol. Chem. 6*, 391-396.

49. O'Donoghue, A. C., Amyes, T. L., and Richard, J. P. (2005) Hydron Transfer Catalyzed by Triosephosphate Isomerase. Products of Isomerization of Dihydroxyacetone Phosphate in D_2O. *Biochemistry 44*, 2622-2631.

50. O'Donoghue, A. C., Amyes, T. L., and Richard, J. P. (2005) Hydron Transfer Catalyzed by Triosephosphate Isomerase. Products of Isomerization of (R)-Glyceraldehyde 3-Phosphate in D_2O. *Biochemistry 44*, 2610-2621.

51. O'Connor, E. J., Tomita, Y., and McDermott, A. E. (1994) Synthesis of (1,2-$^{13}C_2$)-2-phosphoglycolic acid. *J. Labelled Compd. Radiopharm. 34*, 735-740.

52. Bergemeyer, H. U., Haid, E., and Nelboeck-Hochstetter, M. (1972) Process for preparing open ring tetrose and triosephosphate acetals and phosphate ketals, (Office, U. P., Ed.), US.

53. Zhai, X., Amyes, T. L., Wierenga, R. K., Loria, J. P., and Richard, J. P. (2013) Structural Mutations That Probe the Interactions between the Catalytic and Dianion Activation Sites of Triosephosphate Isomerase. *Biochemistry 52*, 5928-5940.

54. Desai, K. K., and Miller, B. G. (2008) A Metabolic Bypass of the Triosephosphate Isomerase Reaction. *Biochemistry 47*, 7983-7985.

55. Gasteiger, E., Hoogland, C., Gattiker, A., Duvaud, S., Wilkins, M. R., Appel, R. D., and Bairoch, A. (2005) Protein identification and analysis tools on the ExPASy server. *Proteomics Protoc. Handb.*, 571-607.

56. Hermes, J. D., Parekh, S. M., Blacklow, S. C., Koster, H., and Knowles, J. R. (1989) A reliable method for random mutagenesis: the generation of mutant libraries using spiked oligodeoxyribonucleotide primers. *Gene 84*, 143-151.

57. Straus, D., and Gilbert, W. (1985) Chicken triosephosphate isomerase complements an Escherichia coli deficiency. *Proc. Natl. Acad. Sci. 82*, 2014-2018.

58. Otwinowski, Z., and Minor, W. (1997) *Processing of X-ray Diffraction Data Collected in Oscillation Mode*, Vol. 276: Macromolecular Crystallography, Part A, Academic Press, New York.

59. Zhang, Z., Sugio, S., Komives, E. A., Liu, K. D., Knowles, J. R., Petsko, G. A., and Ringe, D. (1994) Crystal structure of recombinant chicken triosephosphate isomerase-phosphoglycolohydroxamate complex at 1.8-A resolution. *Biochemistry 33*, 2830-2837.

60. Bailey, S. (1994) The Ccp4 Suite - Programs for Protein Crystallography. *Acta Crystallogr D 50*, 760-763.

61. Delaglio, F., Grzesiek, S., Vuister, G., Zhu, G., Pfeifer, J., and Bax, A. (1995) NMRPipe: A multidimensional spectral processing system based on UNIX pipes. *J. Biomol. NMR 6*, 277-293.

62. Goddard, T., and Kneller, D.G. . SPARKY 3, University of California, San Francisco, CA.

63. Loria, J. P., Rance, M., and Palmer, A., III. (1999) A TROSY CPMG sequence for characterizing chemical exchange in large proteins. *J. Biomol. NMR 15*, 151-155.

64. Loria, J. P., Rance, M., and Palmer III, A. G. (1999) Transverse-Relaxation-Optimized (TROSY) Gradient-Enhanced Triple-Resonance NMR Spectroscopy. *J. Mag. Res. 141*, 180-184.

65. Wittekind, M., and Mueller, L. (1993) HNCACB, a High-Sensitivity 3D NMR Experiment to Correlate Amide-Proton and Nitrogen Resonances with the Alpha- and Beta-Carbon Resonances in Proteins. *J. Mag. Res., Ser B 101*, 201-205.

66. Kay, L. E., Ikura, M., Tschudin, R., and Bax, A. (1990) 3-Dimensional Triple-Resonance NMR-Spectroscopy of Isotopically Enriched Proteins. *J. Mag. Res. 89*, 496-514.

67. Grzesiek, S., Stahl, S. J., Wingfield, P. T., and Bax, A. (1996) The CD4 Determinant for Downregulation by HIV-1 Nef Directly Binds to Nef. Mapping of the Nef Binding Surface by NMR. *Biochemistry 35*, 10256-10261.

68. Hernandez-Alcantara, G., Rodriguez-Romero, A., Reyes-Vivas, H., Peon, J., Cabrera, N., Ortiz, C., Enriquez-Flores, S., De la Mora-De la Mora, I., and Lopez-Velazquez, G. (2008) Unraveling the mechanisms of tryptophan fluorescence quenching in the triosephosphate isomerase from Giardia lamblia. *Biochim Biophys Acta 1784*, 1493-1500.

69. Nickbarg, E. B., and Knowles, J. R. (1988) Triosephosphate isomerase: energetics of the reaction catalyzed by the yeast enzyme expressed in Escherichia coli. *Biochemistry 27*, 5939-5947.

70. Wolfenden, R. (1969) Transition state analogues for enzyme catalysis. *Nature 223*, 704-705.

71. Malabanan, M. M., Koudelka, A. P., Amyes, T. L., and Richard, J. P. (2012) Mechanism for Activation of Triosephosphate Isomerase by Phosphite Dianion: The Role of a Hydrophobic Clamp. *J. Am. Chem. Soc. 134*, 10286–10298.

72. Malabanan, M. M., Go, M., Amyes, T. L., and Richard, J. P. (2011) Wildtype and Engineered Monomeric Triosephosphate Isomerase from Trypanosoma brucei: Partitioning of Reaction Intermediates in D_2O and Activation by Phosphite Dianion. *Biochemistry 50*, 5767-5679.

73. Malabanan, M. M., Amyes, T. L., and Richard, J. P. (2011) Mechanism for Activation of Triosephosphate Isomerase by Phosphite Dianion: The Role of a Ligand-Driven Conformational Change. *J. Am. Chem. Soc. 133*, 16428-16431.

74. Go, M. K., Malabanan, M. M., Amyes, T. L., and Richard, J. P. (2010) Bovine Serum Albumin-Catalyzed Deprotonation of [1-^{13}C]Glycolaldehyde: Protein Reactivity toward Deprotonation of the α-Hydroxy α-Carbonyl Carbon. *Biochemistry 49*, 7704-7708.

75. Malabanan, M. M., Go, M. K., Amyes, T. L., and Richard, J. P. (2011) Wildtype and Engineered Monomeric Triosephosphate Isomerase from Trypanosoma brucei: Partitioning of Reaction Intermediates in D2O and Activation by Phosphite Dianion. *Biochemistry 50*, 5767-5779.

76. Go, M. K., Malabanan, M. M., Amyes, T. L., and Richard, J. P. (2010) Bovine Serum Albumin-Catalyzed Deprotonation of [1-^{13}C]-Glycolaldehyde: Protein Reactivity toward Deprotonation of α-Hydroxy α-Carbonyl Carbon. *Biochemistry 49*, 7704-7708.

77. Kursula, I., Salin, M., Sun, J., Norledge, B. V., Haapalainen, A. M., Sampson, N. S., and Wierenga, R. K. (2004) Understanding protein lids: structural analysis of active hinge mutants in triosephosphate isomerase. *Protein Engineering, Design & Selection 17*, 375-382.

78. Dougherty, D. A. (2013) The Cation-pi Interaction. *Acc. Chem. Res. 46*, 885-893.

79. Walden, H., Taylor, G., Lilie, H., Knura, T., and Hensel, R. (2004) Triosephosphate isomerase of the hyperthermophile Thermoproteus tenax: thermostability is not everything. *Biochem. Soc. Trans. 32*, 305-305.

80. Walden, H., Bell, G. S., Russell, R. J. M., Siebers, B., Hensel, R., and Taylor, G. L. (2001) Tiny TIM: A small, tetrameric, hyperthermostable triosephosphate isomerase. *J. Mol. Biol. 306*, 745-757.

81. Gayathri, P., Banerjee, M., Vijayalakshmi, A., Azeez, S., Balaram, H., Balaram, P., and Murthy, M. R. N. (2007) Structure of triosephosphate isomerase (TIM) from Methanocaldococcus jannaschii. *Acta Crystallogr D Biol Crystallogr 63*, 206-220.

82. Xiang, J., Sun, J., and Sampson, N. S. (2001) The importance of hinge sequence for loop function and catalytic activity in the reaction catalyzed by triosephosphate isomerase. *J. Mol. Biol. 307*, 1103-1112.

83. Zhai, X., Malabanan, M. M., Amyes, T. L., and Richard, J. P. (2014) Mechanistic imperatives for deprotonation of carbon catalyzed by triosephosphate isomerase: enzyme activation by phosphite dianion. *J. Phys. Org. Chem. 27*, 269-276.

84. Zhai, X., Amyes, T. L., and Richard, J. P. (2014) Enzyme Architecture: Remarkably Similar Transition States for Triosephosphate Isomerase-Catalyzed Reactions of the Whole Substrate and the Substrate in Pieces. *J. Am. Chem. Soc.*, 140306071836005.

85. Lolis, E., and Petsko, G. A. (1990) Crystallographic analysis of the complex between triosephosphate isomerase and 2-phosphoglycolate at 2.5-Å resolution: implications for catalysis. *Biochemistry 29*, 6619-6625.

Table 1. Kinetic Parameters for Isomerization Reactions of GAP and DHAP Catalyzed by Wild Type *c*TIM, a Loop 6 Deletion Mutant and a Loop 6 Replacement Mutant.[a]

Enzyme	Substrate	k_{cat} (s^{-1})	K_m (M)	k_{cat}/K_m ($M^{-1}s^{-1}$)	K_i (M)
Wildtype [b]	**GAP**	3200	2.9×10^{-4}	1.1×10^{7}	1.9×10^{-5} PGA
	DHAP	340	5.9×10^{-4}	5.8×10^{5}	
L6RM [c]	**GAP**	> 20 [d]	> 0.04	470	> 0.04 [e]
	DHAP			20	
LDM [f]	**GAP**	0.030 (0.045)	2.1×10^{-3} (2.3×10^{-3})	14 (20)	(1.5×10^{-3}) PGH

[a] Under standard assay conditions: 30 mM TEA buffer, pH 7.5, I = 0.1 (NaCl) and 25 °C [b] Data from ref 53. [c] Determined as the slope of the linear portion ([S] < 3 mM) of the correlations shown in Figures 4A and 4B. [d] Calculated with the assumption that GAP and PGA show a similar weak affinity for the L6RM, by combining the lower limit of K_m > 40 mM from the text with $k_{cat}/K_m = 470\ M^{-1}\ s^{-1}$. [e] A lower limit of K_i for PGA, calculated if 10 mM PGA caused undetected 20% decrease in k_{cat}/K_m for the L6RM-catalyzed isomerization of GAP. [f] The kinetic parameters in parentheses are for the LDM-catalyzed isomerization at 30 °C reported in Ref 28.

Table 2. Product Distributions and Partition Rate Constant Ratios for the Reaction of GAP in D_2O Catalyzed by Wildtype and Loop 6 Mutants of *c*TIM.[a]

Enzyme	k_{obs} [b] (s^{-1})	f_{DHAP} [c]	$f_{d\text{-}DHAP}$ [c]	$f_{d\text{-}GAP}$ [c]	$(f_{MG})_{obs}$ [c]	$(f_{MG})_E$ [d]
L6RM 0.4 μM	2.7×10^{-4}	0.05	0.09	0.83	0.04	0
Normalized product yields $(f_P)_E$ [e]		0.05	0.09	0.86		
LDM 7 μM	7.5×10^{-5}	0.01	0.02	0.22	0.75	0.52
Normalized product yields $(f_P)_E$ [e]		0.04	0.08	0.88		

Partition Rate Constant Ratios [f]	
Wildtype [g]	$(k_{C1})_H/k_{ex} = 0.96$ $(k_{C1})_D/(k_{C2})_D = 1.48$
L6RM	$(k_{C1})_H/k_{ex} = 0.05$ $(k_{C1})_D/(k_{C2})_D = 0.10$
LDM	$(k_{C1})_H/k_{ex} = 0.04$ $(k_{C1})_D/(k_{C2})_D = 0.09$

[a] For the reaction of 10 mM GAP in D_2O buffered by 10 mM imidazole at pD 7.9 and I = 0.10 (NaCl). [b] Observed rate constant for the disappearance of GAP. [c] Determined by extrapolation of plots of observed normalized product yields $(f_P)_{obs}$ against time, to zero reaction time. [d] The difference between the observed yield of MG, and the estimated yield from the nonenzymatic elimination. [e] Normalized yield of products from proton transfer reactions at the active site of TIM, calculated from the observed yields using eq 7 – 9. [f] Rate constant ratios defined by eqs 11 and 12. [g] Data from ref 50.

Table 3. Kinetic Data for the Reaction of [1-^{13}C]-GA Catalyzed by the LDM and the L6RM of *c*TIM in D_2O in the Absence and Presence of HP_i.[a]

Enzyme	$[HPO_3^{2-}]$/mM	[TIM]/M	k_{obs} [b] (s^{-1})	$(k_{cat}/K_m)_{obs}$ [c] ($M^{-1}\ s^{-1}$)	$\frac{k_{cat}}{K_{HPi}K_{GA}}$ [d] ($M^{-2}\ s^{-1}$)
LDM	0	3.2×10^{-4}	2.6×10^{-6}	0.14	
	20.0	3.2×10^{-4}	4.0×10^{-6}	0.22	≤ 0.25 [e]
L6RM	0	3.9×10^{-4}	2.7×10^{-6}	0.11	
	20.0	2.3×10^{-4}	3.4×10^{-6}	0.25	0.50 [f]

[a] For reactions of 20 mM [1-^{13}C]-GA in D_2O at pD 7.0 (10 mM imidazole), and I = 0.1 (NaCl). [b] Observed first-order rate constant for the reactions of [1-^{13}C]-GA calculated based on eq 1. [c] Second-order rate constant for the *c*TIM-catalyzed reactions of [1-^{13}C]-GA calculated based on eq 2. [d] The estimated third-order rate constant for the HP_i activated *c*TIM-catalyzed reactions of [1-^{13}C]-GA calculated based on eq 10. [e] The upper limit for $\frac{k_{cat}}{K_m K_{HPi}}$, which could have been detected in these experiments, shown as the horizontal dotted line in Figure 8. [f] Estimated as described in the text.

FIGURE LEGENDS

Figure 1. Models which show representations of the X-ray crystal structures for wild type TIM and a loop 6 deletion mutant (LDM). (A) Space filling model of the complex between TIM from yeast and PGA [PDB entry 2YPI].[85] The amino acid side chains of loop 6 that were retained for the LDM are shaded magenta, and the deleted residues are shaded green. The cationic side chain of K12 is shown with the nitrogen (blue) in an ion pair to oxygen (red) of the anionic side chain of E97. (B) The LDM of *c*TIM generated from the structure for wildtype *c*TIM by a procedure similar to that described for the K12G mutant of TIM from yeast.[26] The amino acid side chains of loop 6 that were retained for the LDM are shaded magenta. Reprinted with permission from Ref 17. Copyright 2012 American Chemical Society. In solution TIM exists as a homodimer. Here we show only the monomer for clarity.

Figure 2. A summary of the effect of the L6RM on the NMR chemical shifts of backbone amides resonances, for spectra acquired at 14.1 T, 298 K and pH 6.6. (A) A superposition of the resonances for wildtype (red) and L6RM (blue) TIM at the unliganded enzymes. (B) The values of d^{NH} (ppm) for the L6RM mutation, where d^{NH} is the effect of the L6RM on the composite chemical shift, as defined by eq 3. (C) A model for wildtype *c*TIM, which shows the positions in the protein structure where the L6RM was found to result in significant values for d^{NH} (> 0.2 ppm). The structure has been coded to match the colors shown by the dashed line in Figure 2B with blue residues highlighted by circles. The side chains of the two mutated residues are depicted. The position of active site and loop-6 are indicated to orient the viewer.

Figure 3. A summary of the effect of the binding of G3P to wild type *c*TIM and to the L6RM on the NMR chemical shifts of backbone amide resonances, for spectra acquired at 14.1 T, 298 K and pH 6.6. (Panels A and B) Superposition of signals for wild type *c*TIM (panel A) or the L6RM (panel B) in the unliganded (red) and G3P saturated (blue) forms. The inset shows the titration profile for residues 168, 177, and 212. The arrows indicate the direction of the shift in the resonance as the unliganded enzyme is saturated by G3P. (Panels C and D) The values of δ^{NH} (ppm) observed upon saturation of wildtype *c*TIM (panel C) and the L6RM (panel D) by G3P, where δ^{NH} is the effect of ligand binding on chemical shift. (Panels E and F) A model for wild type *c*TIM (PDB entry 1TIM), which shows, in red, the position in the protein structure where the binding of G3P results in significant values for δ^{NH} (> 0.1 ppm) for wild type *c*TIM (panel E) or the L6RM (panel F). The site of the mutation is shown in green in panel F

Figure 4. Michaelis-Menten plot of initial velocity data for the isomerization of GAP and DHAP catalyzed by the L6RM of *c*TIM at pH 7.5 (30 mM TEA buffer), 25 ºC, I = 0.1 (NaCl). The solid line shows the fit of data to the Michaelis-Menten equation, and the dashed line is the linear relationship of the data at low concentration of substrate ([S] ≤ 3 mM). The inset shows the linear correlation of the initial velocity data for ≤ 3 mM [GAP] or [DHAP], the slope of which gives the second order rate constant k_{cat}/K_m.

Figure 5. Rate and product data for the reactions of GAP (10 mM) in D_2O catalyzed by 0.4 μM of the L6RM (Figures 6A and 6B) and by 7 μM of the LDM (Figures 6C and 6D) of *c*TIM, determined by ^{1}H NMR spectroscopy.[50] Figures 6A and 6C: The decrease in the fraction of GAP (f_{GAP}) remaining for reactions catalyzed by the L6RM and LDM of *c*TIM, respectively. Figures

6B and 6D: The fractional product yields, $(f_P)_{obs}$, (eq 4) for reactions catalyzed by the L6RM and LDM of *c*TIM, respectively. Key - (Figure 5B): (●), $(f_{d\text{-DGAP}})_{obs}$; (■), $(f_{d\text{-DHAP}})_{obs}$; (▲), $(f_{DHAP})_{obs}$. (Figure 5D): (▼), $(f_{MG})_{obs}$; (●), $(f_{d\text{-DGAP}})_{obs}$; (■), $(f_{d\text{-DHAP}})_{obs}$; (▲), $(f_{DHAP})_{obs}$.

Figure 6. Representations of X-ray crystal structures of TIM in the region of the N-terminal hinge of loop 6. (A) Wild type *c*TIM (PDB entry 1TIM). (B) Wild type *c*TIM liganded to PGH (PDB entry 1TPH). (C) Superimposed X-ray crystal structures of unliganded *c*TIM in the region of the N-terminal hinge: blue ribbon, wild type cTIM (PDB entry ITIM); green ribbon, unliganded L6RM of *c*TIM (PDB entry 4P61). Monomer B, shown for the L6RM, has no significant electron density from residues 173 – 175. (D) TIM from *Pyrococcus woesei* liganded to 3-phosphonopropanoic acid (PDB entry 1HG3). The carboxylate side chain of the hinge residue E147, which occupies a position equivalent to that of W168 from *c*TIM, is stabilized by a hydrogen bond to the cationic side chain of K159.

Figure 7. A Scheme with shows the minimal mechanism for the TIM-catalyzed reactions of GAP in D_2O that results in the formation of *h*-DHAP, *d*-DHAP and *d*-GAP. The -H derived from substrate may exchanged with a pool of deuterium at the enzyme. There is evidence that the transfer of hydrogen between O-1 and O-2 of the enediolate reaction intermediate is mediated by the imidazole side chain of His-95.[11]

Figure 8. Linear free energy relationship, with a slope of 1.04 ± 0.03, between logarithmic values of second-order rate constants [log $(k_{cat}/K_m)_{GAP}$] for wildtype and mutant TIM-catalyzed isomerization of GAP and the third-order rate constants [log $(k_{cat}/K_{HPi}K_{GA})$] for wild type and

mutant TIM-catalyzed reactions of the substrate pieces GA and HP_i (Scheme 5). Most of these data were reported and discussed in an earlier publication.[84] The dotted line shows an estimate for the smallest third-order rate constant $k_{cat}/K_{HPi}K_{GA}$ that could have been detected by our experimental methods. Key for mutants of TIM: Green, TIM from *Trypanosoma brucei*; red, TIM from chicken muscle; blue, TIM from yeast.

Figure 1
Zhai et al.

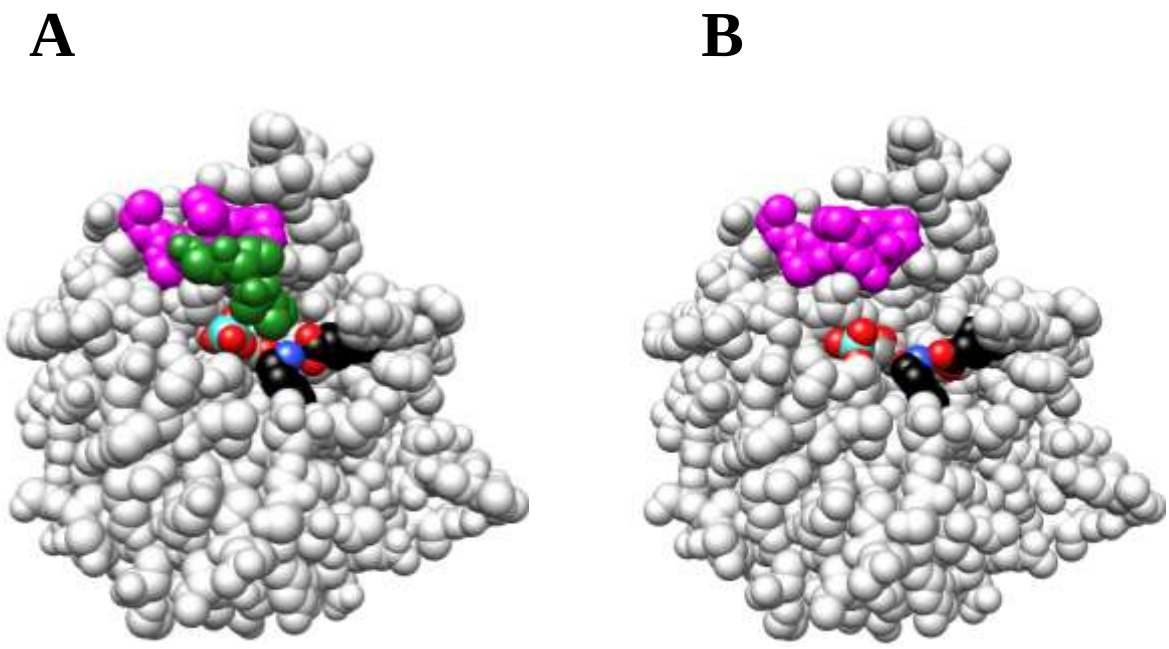

Figure 2
Zhai et al.

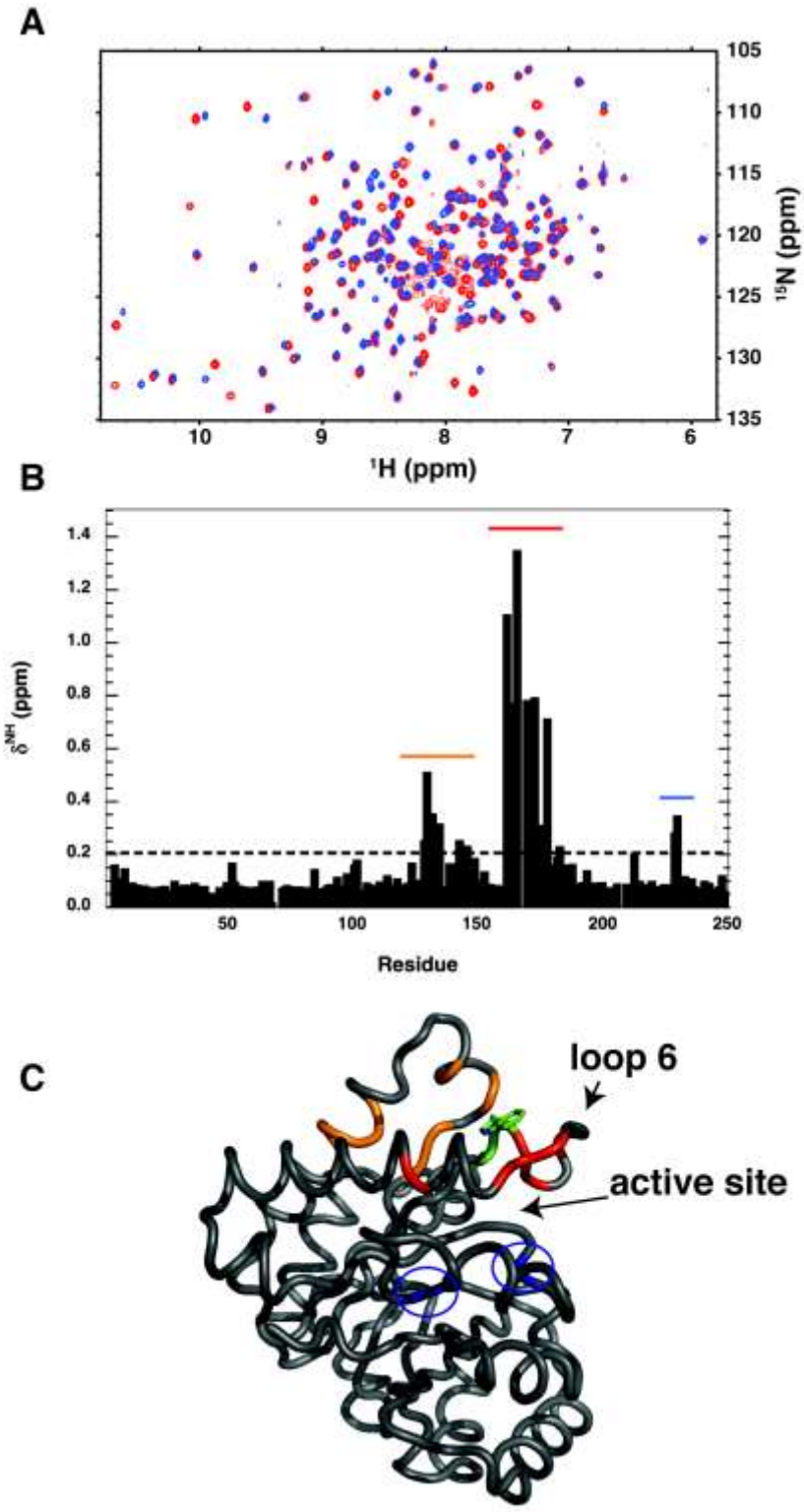

Figure 3
Zhai et al.

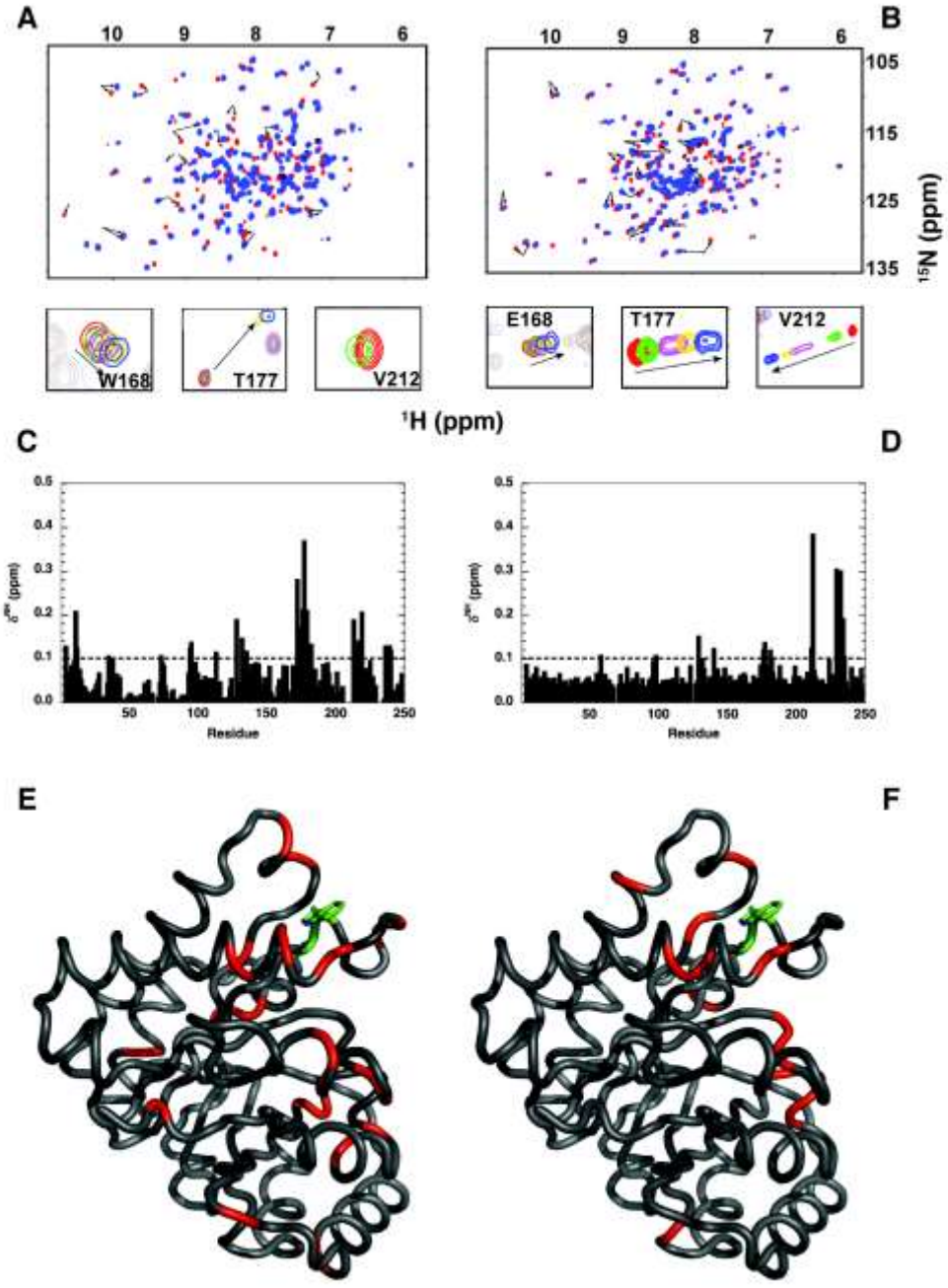

Figure 4
Zhai et al.

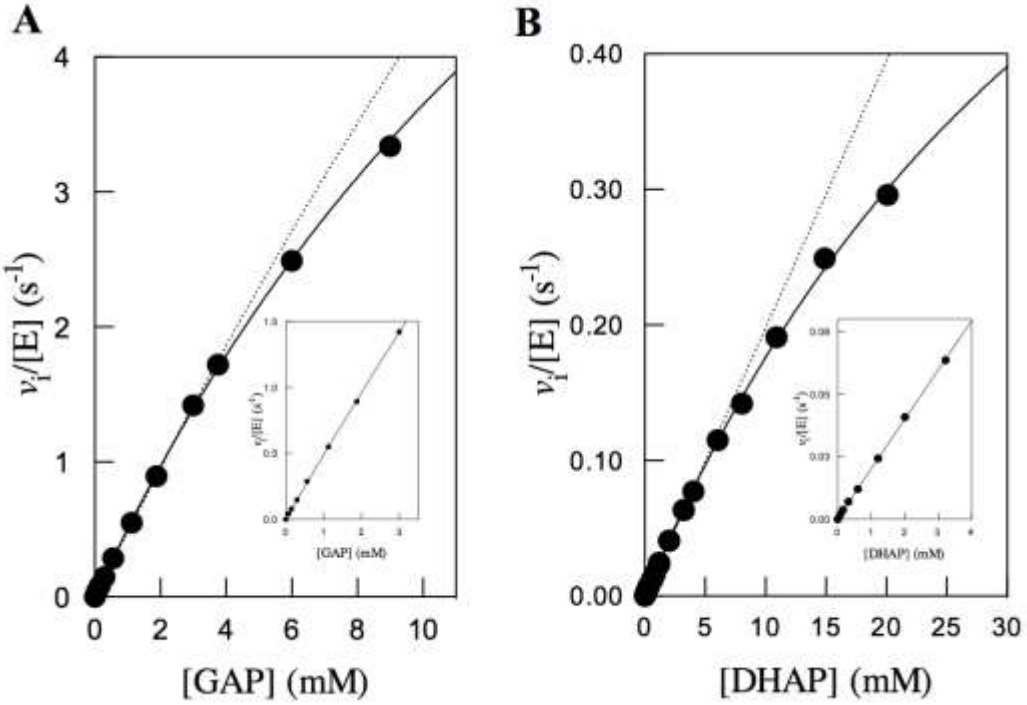

Figure 5
Zhai et al.

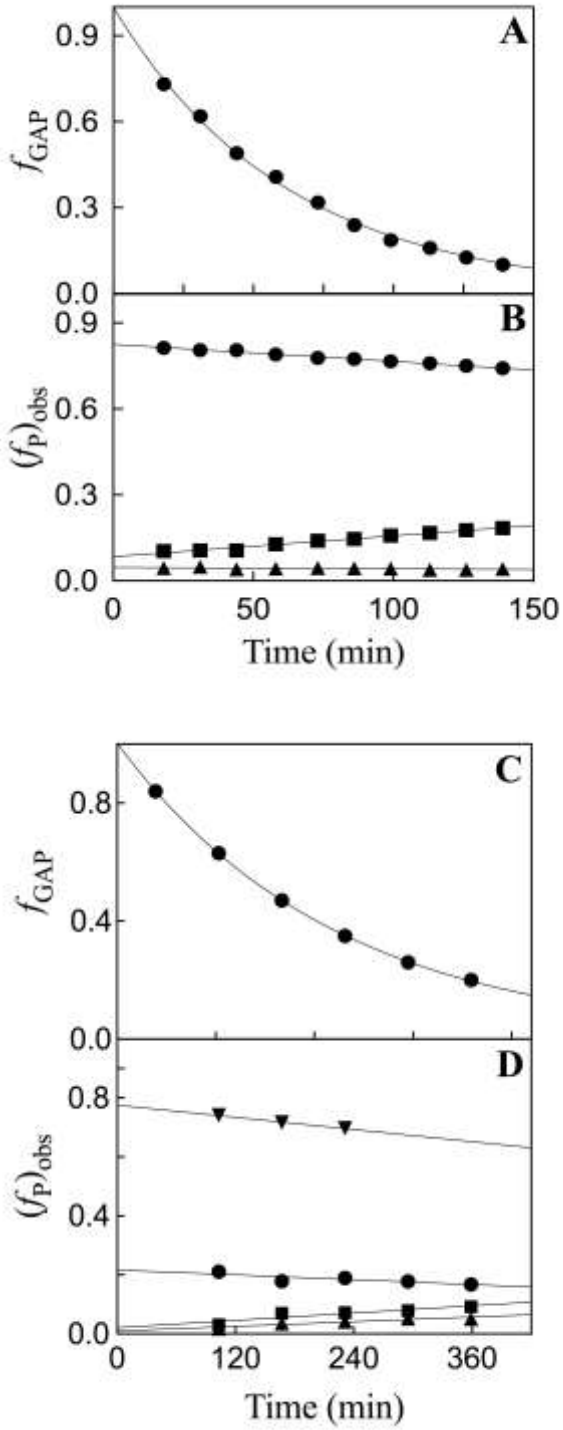

Figure 6
Zhai et al.

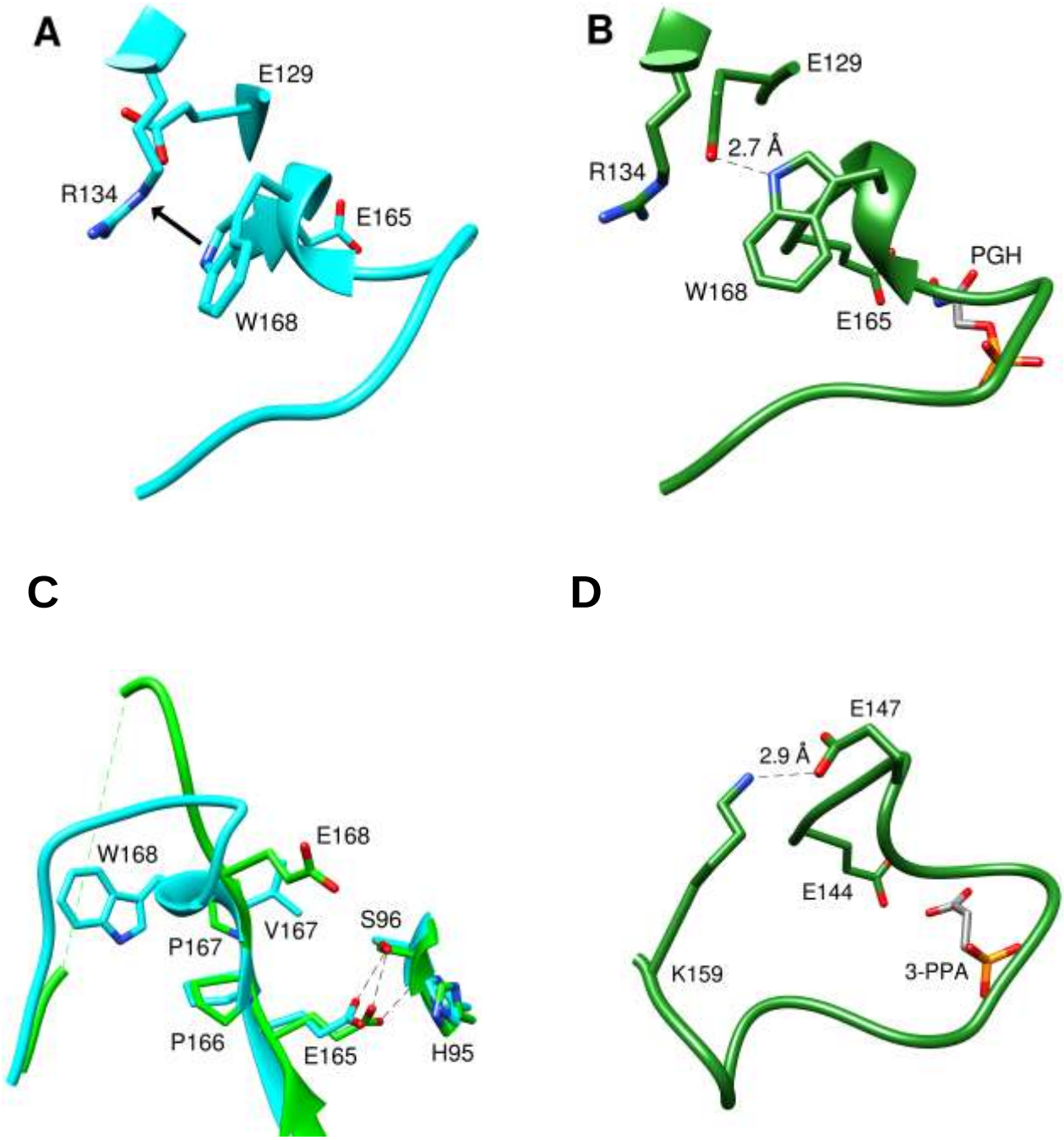

Figure 7
Zhai et al.

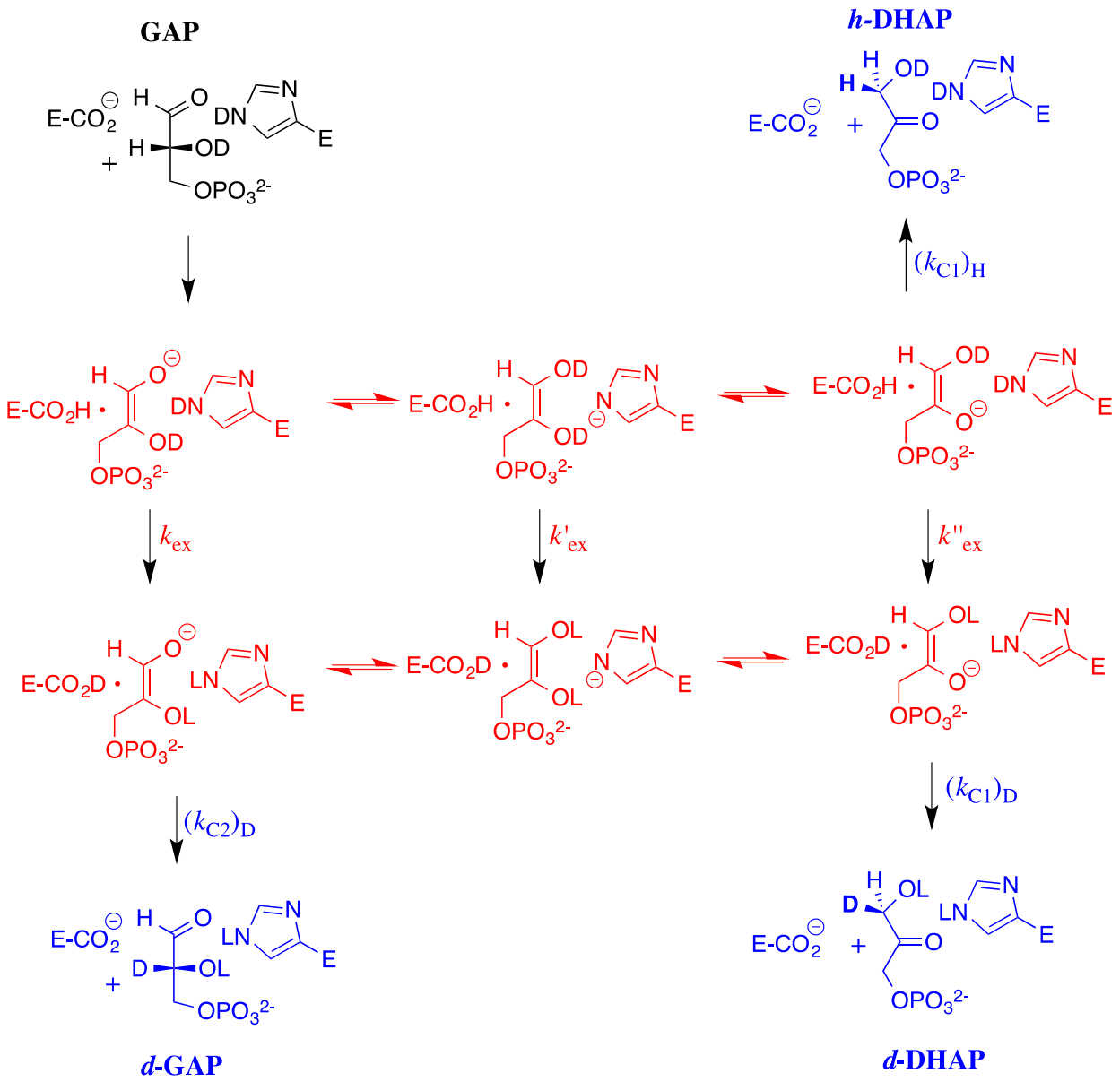

Figure 8
Zhai et al.

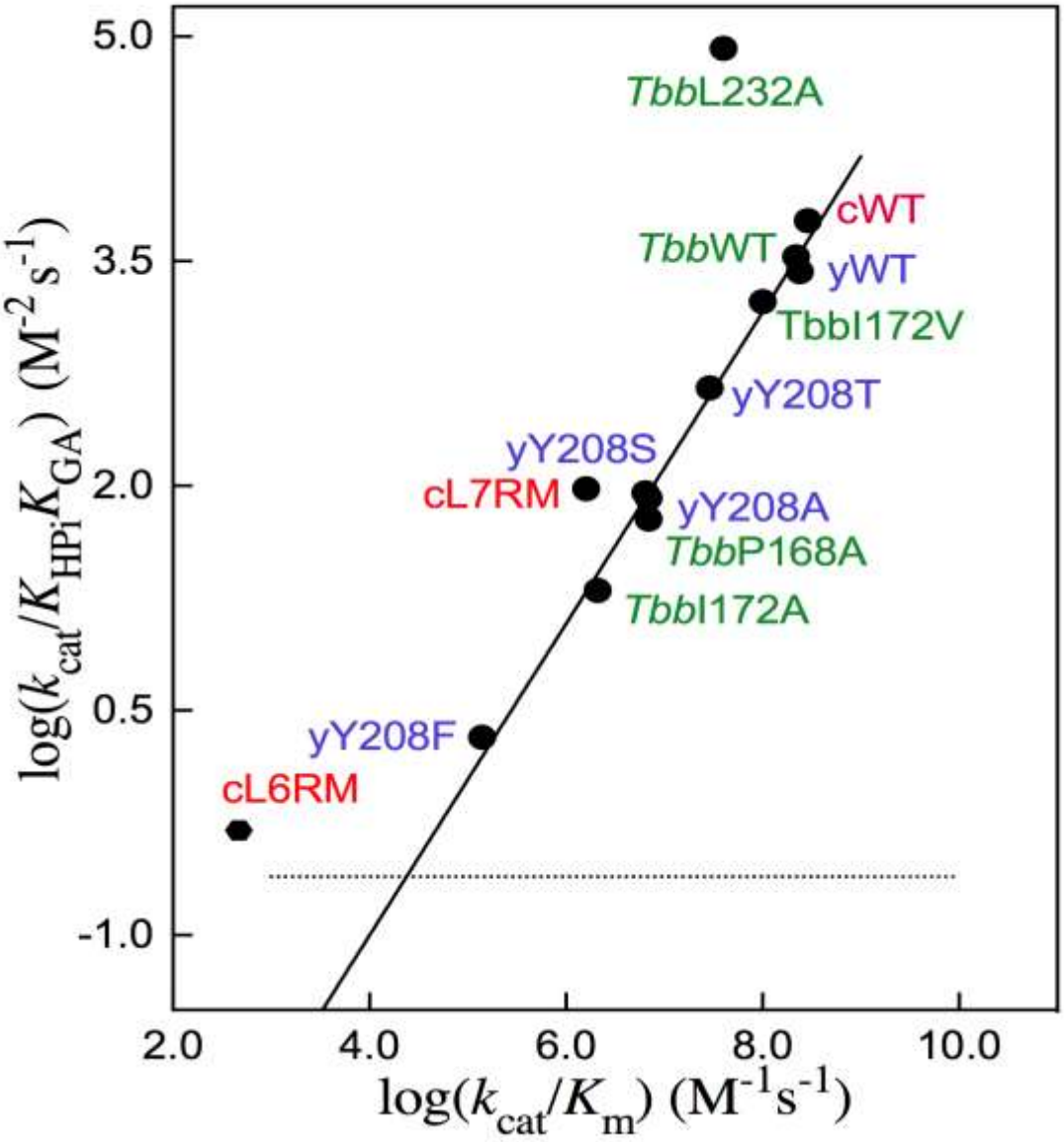

TOC GRAPHIC

[3.5 x 9.0 cm]

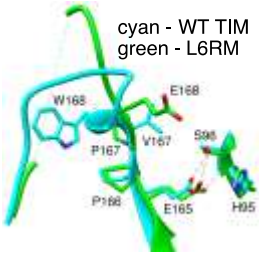

P166 A176

YE-PVW-AIGTG-KTA-TP Wildtype Loop 6

YE-PPE-AIGTG-KTA-TP Loop 6 Mutation

N-Terminal Hinge

C-Terminal Hinge

Loop 6 replacement mutation introduces severe kink into structure of wild type triosephosphate isomerase (TIM). Substrate binding energy is used to eliminate kink from "plastic" enzyme and restore enzyme to active structure.